UCRL-1590

UNIVERSITY OF CALIFORNIA — BERKELEY

RADIATION LABORATORY

DISCLAIMER

UCRL-1590
Unclassified-Physics Distribution

UNCLASSIFIED

UNIVERSITY OF CALIFORNIA

Radiation Laboratory

Contract No. W-7405-eng-48

DEUTERON PHOTODISINTEGRATION AT HIGH ENERGIES

William Gilbert

(Thesis)

December 7, 1951

Berkeley, California

TABLE OF CONTENTS

TABLE OF CONTENTS (CONT.)

DEUTERON PHOTODISINTEGRATION AT HIGH ENERGIES

William Gilbert

Radiation Laboratory, Department of Physics
University of California, Berkeley, California

December 7, 1951

I ABSTRACT

The reaction $\gamma + D \rightarrow p + n$ was investigated using the photon bremsstrahlung spectrum from the Berkeley electron synchrotron which has a quantum limit of approximately 320 Mev. The target consisted of deuterium gas at a pressure of 2000 P.S.I. and at a temperature of 77° K. Protons were detected by a scintillation counter telescope system consisting of three liquid phosphors viewed by several photomultiplier tubes each. The outputs from these counters were pulse height discriminated and then the pulses of the proper height were fed into coincidence circuits in such a manner that the detection system was specific in its acceptance of proton events and in its rejection of meson events. The energy of a proton accepted by the system could be determined by the use of absorbers in front of the counter telescope and the angular and energy resolution of the system was sufficient to define the energy of the initial γ-ray to a few Mev.

$\left(\frac{d\sigma}{d\Omega}\right)_\theta$ were determined at laboratory angles of 30°, 45°, 60°, 75°, and 90° for E_γ center of mass = 200 ± 15 Mev, and at laboratory angles of 30°, 45°, 60°, 75°, 90°, 105°, 115° for E_γ center of mass = 250 ± 15 Mev.

$$\sigma \text{ total (200 Mev)} = (10.0 \pm 3.0) \times 10^{-29} \text{ cm}^2$$

$$\sigma \text{ total (250 Mev)} = (15.9 \pm 6.4) \times 10^{-29} \text{ cm}^2$$

These cross sections are far greater than reasonable extrapolations of theoretically predicted cross sections at lower photon energies could yield. These data indicate that above the threshold for the production of mesons, the cross section for the photoeffect rises with increasing photon energy and that around this energy, 140 Mev, the cross section is larger than theories which exclude the effects of meson interaction can predict.

DEUTERON PHOTODISINTEGRATION AT HIGH ENERGIES

William Gilbert

Radiation Laboratory, Department of Physics
University of California, Berkeley, California

December 7, 1951

II INTRODUCTION

The deuteron, by virtue of being a two body system, is of primary interest in nuclear theory since one might hope to solve its wave equations exactly. Ever since the theoretical papers of Bethe and Peierls[1], Fermi[2], and Bethe and Bacher[3], relating to the photodisintegration of the deuteron and its inverse reaction, the n-p capture process, numerous experimental studies have been carried out to test the theory and to determine specific parameters relating to the deuteron's binding energy, the shape, width and depth of the nuclear potential well as well as to other associated problems. The overwhelming bulk of these investigations has been carried out with naturally radioactive γ-emitters, none of which have γ's of over a few Mev energy. Recently, work has been carried to approximately 20 Mev[4,5]. The primary conclusions one draws from the experiments done at these energies relate to the effective ranges and to the binding energies in the various deuteron states.

Various theoretical calculations have been carried out for γ-energies up to 300 Mev[6,7,8]. The more detailed of these calculations use the best parameters derived from other work like n-p scattering and are carried out to a γ-energy of 150 Mev. Effects due to exchange forces, other specifically mesonic interactions, and higher order multipoles,

would become important, if at all, only at energies very much higher than the previous experimental limit of approximately 20 Mev.

The Berkeley synchrotron yields photons of energies (center of mass) up to about 280 Mev and for reasons stated above, it appeared desirable to investigate the photoeffect at these high energies.

Since the current theoretical predictions are based on a long extrapolation of data taken at low photon energy, data taken from n-p scattering, and the exclusion of specifically mesonic contributions, the predicted cross sections at these high energies might be considered as being suspect. Experimental cross sections at these high energies should serve to test the validity of the assumptions used. In addition one could reasonably expect to discover the magnitude of the contributions made to the cross section by the meson interaction.

III DESCRIPTION OF THE EXPERIMENT

The x-rays were produced in the Berkeley electron synchrotron by letting the 298-324 Mev electron beam strike a 0.020 inch platinum target placed on the inner side of the accelerating tube. The "spread-out" bremstrahlung beam was obtained by modulating the rf accelerating voltage such that the electrons spill into the target over a period of about 3,000 μ sec. The emerging beam had a full width at half intensity of 0.0135 radians. (See Figure 1.) At 55 inches from the platinum target, the beam was collimated by a tapered hole in a lead block nine inches thick. The collimating hole was 0.50 inch in diameter at the entrance end and was part of a cone whose apex lay at the platinum target. Directly behind the primary collimator was the secondary collimator which was of lead and was six inches long and had a one-inch hole. Behind this and directly in front of the experimental target was a collimator of lead, six inches thick and with a 2-inch hole. The target and collimators were aligned by means of a transit. Photographs of the beam were taken with a 1/8 inch primary collimator and the target was aligned with respect to this small, well defined beam. Then the larger primary collimator was inserted. At the end of the experiment the 1/8 inch collimator was replaced and photographs were again taken. The target proved to be aligned at the end of the run.

The experiment was done in two parts. The first was the calibration of the two proton telescopes such that protons would be counted and mesons rejected. For this purpose a 3/4 inch thick carbon target 45°

to the beam direction and 45° to the telescope directions was used (telescopes were at 90° to the beam). The number of protons and mesons per unit beam from such a target was far greater than that which could be expected from the small mass of deuterium in the pressure target and so was useful in counter calibration.

After the proper operating conditions for the electronics were established, the carbon target was removed and the deuterium pressure target was inserted. (Shown in place in Figure 1.) The telescopes were placed at the desired angles to the beam and appropriate absorbers were inserted to correspond to incident γ-ray energies (center of mass) of 200 and 250 Mev. Counting rates were also taken with the deuterium pumped out of the target, for purposes of determining background from the target assembly. The no gas counting rate, although small, was by no means negligible and appropriate corrections were made.

A. Target Assembly

Two types of targets were considered for this experiment. Heavy water used in conjunction with light or ordinary water was first considered for reasons of its simplicity, low cost, and high density of deuterium. The plan was to count the protons from the heavy water and then from the light water and to subtract the latter number from the former. The justification for this is that it is known that the cross section for photoprotons from hydrogen, or Compton protons, is negligible compared with that for oxygen. Therefore it was concluded that the entire counting rate from regular water could be considered as due to the oxygen present. Subtracting this number from the counting rate due to heavy water yields the

deuterium contributions alone. The difficulty arises in the fact that the cross section for photoprotons from oxygen is several times larger than that from deuterium and the statistics of the subtraction are extremely unfavorable.

The alternative was the use of a high pressure, low temperature deuterium target. Although the density of the deuterium was less than that of heavy water, and the counting rate subsequently reduced, the elimination of a subtraction made the problem statistically far more favorable. It is estimated that for identical statistical weight the use of the gas target required about one fifth (1/5) the machine time than would be required by the $D_2O - H_2O$ subtraction. One disadvantage is that the walls of the gas target force one to examine higher energy protons since they act as absorbers.

The assembly of the target is shown in Fig. 2. The target is the one designed and used by R. S. White[9]. The photon beam traversed 0.045 in. of stainless steel on each end of the target, 0.005 inch of vacuum wall and 0.040 inch of pressure wall, all of which represents a thin enough absorber that the beam can be considered to be unaltered. Protons produced in the gas of the target, which were emitted perpendicular to the axis of the target, had to penetrate a 0.080 inch pressure wall, 0.31 inch of liquid nitrogen, a 0.012 inch liquid nitrogen wall, and finally, a 0.027 inch vacuum wall. The equivalent absorber represented by all this is $3.22/\sin\theta$ $gmCu/cm^2$, where θ is the angle between the photon beam to proton directions. This corresponds to protons of 48 Mev at 90° and 71 Mev at 30°. The pressure chamber was hydrostatically tested at room temperature to 240 atmospheres. Gas tests were made at a temperature of 77° K to 340 atmospheres.

In actual usage the pressure never exceeded 150 atmospheres at 77°K so that one always had a tested safety factor of greater than two and a calculated safety factor or greater than four. Three safety pressure patches were inserted in the system (shown in Fig. 3) which would break at 200 atmospheres and allow the gas to expand into the blow off tank, a cylinder of large volume.

The liquid nitrogen was stored in a tank above the target and fed to the cooling wall through pipes. Two thermocouples were placed in the tank at different levels and the signals were sent to an automatic recorder in the counting area so that one had a record of the levels at all times and could fill the tank when necessary. After equilibrium condition had been reached, the nitrogen tank had to be refilled about every two hours. A third thermocouple was placed on one of the end cups so that one also had a record of the temperature of the pressure wall, and thus the gas, at all times.

One high pressure line was led directly from the target to a calibrated pressure gauge in the counting area. At intervals the gas pressure was read from this gauge. The number of target deuterons per cm^3 was obtained from R. S. White[9].

The vacuum system was for the purpose of lowering the heat conduction to the outside wall which was at room temperature, and for conserving the liquid nitrogen in the Dewar. Without this vacuum system the walls of the target would ice to the point that the proton energies would be indeterminate. To obtain the vacuum of about 10^{-6} mm of Hg a 20-liter oil diffusion pump was used, backed by a Duo seal fore

pump. The target, collimators and detectors in their shields are shown in Figs. 4, 5.

B. High Pressure System

The high pressure system is shown schematically in Fig. 3. There are three safety pressure patches and one dumping valve, all four of which lead to a large evacuated cylinder, the blow off tank. In case of excessive pressure in any part of the system, one of these four safety devices allows the deuterium to escape to this low pressure, isolated system. Since it is an isolated system, the deuterium can be recovered at some future time in case of an accident that causes the safety patches to blow. The deuterium pumping system is the one used by R. S. White[9].

C. Collimators, Slits and Shielding

The counters were placed in lead houses in order to be shielded from the general background of electrons and x-rays which pervade the magnet room of the synchrotron. The walls varied in thickness from 2 in. to 4 in. and in most directions were 4 in. A hole in the front wall of the lead house served as one slit in the proton collimator. Since the source of protons was a line target of deuterium, it was necessary to define the target seen by the counters by a two slit collimator system. The front slit was a hole in a copper block. See Figure 4. Lead shielding was used so that only those particles that passed through the front slit could enter the rear slit. This shielding was removed in Figure 4 and 5 so that more detail could be seen. The angular resolution of the collimation system was such that the bulk of the protons accepted were in the angular range $\theta \pm 4^{\circ}$. However a few protons were accepted from between $4^{\circ} - 6^{\circ}$ from θ. Therefore the overall angular resolution was $\pm 6^{\circ}$.

IV PROTON DETECTION AND IDENTIFICATION

A. General

In the x-ray beam from the synchrotron, charged particles of different masses (e, π, p, D and probably T, α) are produced in targets of $Z > 2$. For a deuterium target, we would have the 3 particles, electrons, mesons and protons. Thus the identification of a particular charged particle is complicated by the presence of particles of different masses. Coupled with this fact are two others which must be considered in the choice of a detection system; viz, there is a high ambient background of electrons and scattered x-rays, and the number of charged particles of masses > e produced is small enough per unit beam to demand a large effective solid angle for any proposed counter system. With the exception of the α-particle, all the particles one would be interested in are singly charged. For purposes of identification, the information one would like about a detected particle is: the mass, energy, and angle of emission. The determination of the angle is obvious so we need only discuss the determination of the mass and of the energy.

The specific measurements we can make yield the following physical quantities:

(1) dE/dx

(2) Range

(3) Energy

(4) Momentum

(5) Velocity

Through suitable relations we can solve for the particle's mass and energy using the following pairs of measured quantities.

(a) (1) - (2)

(b) (1) - (3)

(c) (1) - (4)

(d) (2) - (4)

(e) (2) - (5)

(f) (3) - (4)

(g) (3) - (5)

(h) (4) - (5)

Now, consider the particular possible measurements and the reasons for rejecting the least desirable three.

(3) Energy - One can measure the total energy of a particle by using a scintillation counter sufficiently thick to stop the particle and pulse height analyzing the crystal's output, which is proportional to the total energy given up by the particle in the counter. For high energies, one requires an excessively thick crystal. This method requires a very sensitive pulse height analysis and at the present time the technique of pulse height analysis is not at an advanced enough state to yield the energy with sufficient accuracy.

(4) Momentum - One measures the momentum of a particle by the use of its $H\rho$ in a magnetic field. The use of such a magnet results in a small effective solid angle and thereby in a small counting rate.

(5) Velocity - The time of flight method depends upon two counters separated by some distance. The velocity resolution is proportional to the separation but the solid angle subtended by the rear counter

is inversely proportional to the square of the separation. The resultant energy resolution is poorand the counting rate small.

(1) dE/dx - (2) Range combination seems to offer the best compromise for sharp energy resolution and large subtended solid angle. The dE/dx shows less dependence upon mass when combined with range than it does when combined with energy or with momentum. Thus the dE/dx must be determined within narrower limits and constitutes one of the major difficulties of the experimental procedure.

B. Scintillation Counter Telescope System

Scintillation rather than gas proportional counters were used because of their greater speed. The counter speed is important because there is a large background of electrons and scattered x-rays which the counter system must be able to reject, although individual counters might record these events as single counts. In order for the system as a whole to reject these extraneous events, the resolving times of the individual counters and the associated coincidence circuits must be short enough to make it improbable that these random single rates will be recorded accidentally as coincidences. Another reason for high speed is that the beam is pulsed which effectively increases the counting rate by the ratio of the total time to the time the beam is on.

The equipment as first used had a resolution and recovery time of about 0.4 μ sec. This is faster than proportional counter equipment is now (about 0.4 - 1 μ sec at best) and much faster than proportional counter equipment was when this experiment was started, over a year ago.

It was discovered that in actual operation the 0.4 μ sec resolving time was not required because of the low accidental rate and we then increased the time to about 1 μ sec. This allowed for greater simplicity in using the electronics. Therefore in practice the speed of our overall counting equipment was not faster than that of the fastest gas proportional counter equipment available today. The limitation was one of choice, namely the type of electronics used and the method in which it was used. The limitation was not one of necessity, i.e., limited by the inherent speed of the counters. In gas proportional counters, the speed is limited by the counter itself to about 0.5 μ sec. The actual pulses coming from our counters were about 10^{-8} sec or 0.01 μ sec long. Therefore, in principle the scintillation counting equipment is much faster than gas proportional counters. In order to utilize this greater speed, the pulses would have to be examined by more refined electronic or photographic means. The photon beam intensities were not such as to cause us to demand greater speed from our counters than the 1 μ sec we used. However, if the beam intensity should rise to the point where the resolving and recovery times of the counting equipment are the limiting factors, one could modify the scintillation system so that it would be much faster than that used in this experiment. Therefore the following statement holds: In a particle detection telescope using dE/dx and range for particle identification, scintillation counters are inherently faster than are gas proportional counters and a system utilizing the former (scintillation) can realize greater speed than one utilizing the latter (gas proportional).

The telescope consisted of three counters as shown on the next page. In order to have large counters, transparent enough not to affect

the pulse height discrimination and of reasonable availability, liquid phosphors were used. It was found that at least two photomultiplier tubes viewing one counter were necessary to yield fairly uniform light collection over the entire region of the counter. For Counter 1 on which the dE/dx was measured, three photomultiplier tubes were used to view the counter.

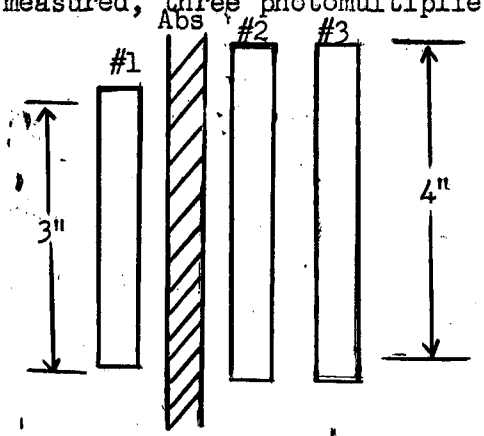

No. 1 = 0.730 in. liquid

Abs = 2.6 gms Cu equiv.

No. 2 = 0.390 in. liquid

No. 3 = 0.500 in. liquid

No. 2 and No. 3 separated by only 0.002 in. Al.

C. Scintillation Counter Telescope as Proportional Counter System

Counter No. 3 is used as an anti-coincidence counter so only those particles that give a pulse in both No. 1 and No. 2 within the resolving time of the system, which is about 1 μ sec, are recorded. Thus we demand that the particle stop in counter No. 2. Consider the following representation for the two extreme cases of an accepted particle:

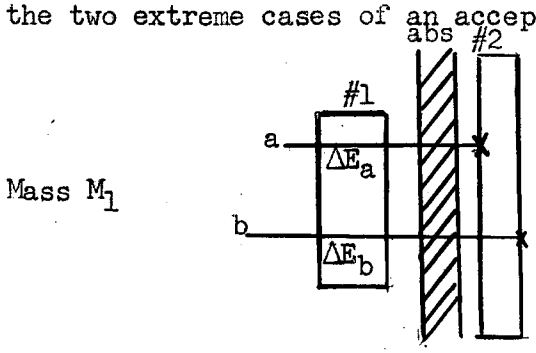

The particle, a, which stops in the front of No. 2 has the largest dE/dx in No. 1 as it is moving slowest in going through No. 1. Since counter No. 1 is thick, a particle's dE/dx changes in traversing it. Rather than use

an average dE/dx, we will use the total energy given up in No. 1, ΔE, which is proportional to $\overline{dE}/dx$. Particle b which stops in the rear of No. 2, gives up the smallest energy to No. 1. Therefore $\Delta E_a > \Delta E_b$. All other particles of this mass give up energies intermediate between these two extremes, $\Delta E_b \leq \Delta E_i \leq \Delta E_a$. The light output in this range of excitation is proportional to the total energy given up by a particle and thus the pulse heights are a measure of these energy losses.

Consider particles of two different masses:

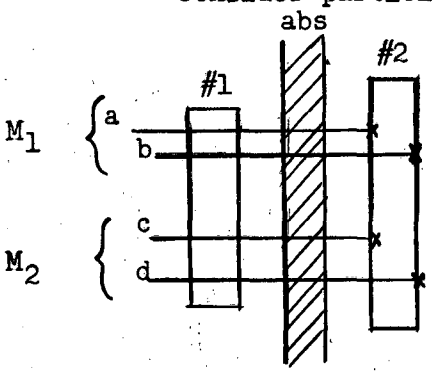

for M_1 $\quad \Delta E_b \leq \Delta E_i \leq \Delta E_a$

for M_2 $\quad \Delta E_d \leq \Delta E_j \leq \Delta E_c$

In order to differentiate between particles of masses M_1 and M_2, it is necessary that the extreme pulse heights for the two cases do not overlap, i.e., $\Delta E_b > \Delta E_c$. It can be shown that the largest possible ratio, if $M_1 > M_2$, is $\frac{\Delta E_b}{\Delta E_c} \cong \left(\frac{M_1}{M_2}\right)^{0.44}$. The larger this ratio, call it merit ratio, the easier is the determination of the mass and identifications of the particle.

$$\text{For } \frac{\text{protons}}{\text{mesons}}, \left(\frac{M_1}{M_2}\right)^{0.44} = \left(\frac{1836}{276}\right)^{0.44} = 2.30$$

$$\frac{\text{deuterons}}{\text{protons}}, \left(\frac{M_1}{M_2}\right)^{0.44} = 2^{0.44} = 1.36$$

For the experimental arrangement above

for protons $\Delta E_a = 20.5$ Mev

$\Delta E_b = 17.0$ Mev

$$\underbrace{62.5 \text{ Mev}}_{E_a} \leq E_p^* \leq \underbrace{71.0 \text{ Mev}}_{E_b}$$

mesons $\Delta E_c = 9.3$ Mev

$\Delta E_d = 8.0$ Mev

$28.0 \text{ Mev} \leq E_\pi^* \leq 32.0 \text{ Mev}$

deuterons $\Delta E_{max} = 28.7$ Mev

$\Delta E_{min} = 24.0$ Mev

$85.0 \text{ Mev} \leq E_{deut}^* \leq 96.5 \text{ Mev}$

Actual merit ratio proton/meson = 17.0/9.3 = 1.83

Actual merit ratio deuteron/proton = 24.0/20.5 = 1.17

* These energies represent the actual total energy required of the particular particle to pass through Counter No. 1, the absorber between No. 1 and No. 2. This gives us the actual energy range the counter selects as well as the energy site, $E_b - E_a$.

The chief reason for the difference between the actual merit ratios and the theoretically limiting ratios is the fact that No. 2 counter must be of finite thickness. With the actual ratios above, it is possible to differentiate mesons from protons, but not to differentiate deuterons from protons. The reasons for this will appear.

D. Pulse Height Discrimination, Effect of Photomultiplier High Voltage, and Ideal Coincidence Plateau.

Let us consider an ideal situation in which only protons and mesons are incident upon our counter system. These particles are of a wide range of energies and we shall only speak about those particles which pass through No. 1 and stop in No. 2. At a given photomultiplier high voltage on No. 1, the pulse height output is proportional to the energy loss of the particle in counter No. 1. The pulse height discriminator acts in such a way as to reject all pulses below the discriminator level and accept all pulses above this level. All the accepted pulses are recorded as events. The discriminator level is kept constant in time. The effect of raising the photomultiplier high voltage is to amplify all pulses proportionately and the photomultiplier high voltage can be considered as analogous to an amplifier gain control. Schematically let us represent the operation of the system in Figure 6. The extreme pulse heights in No. 1 of the protons and mesons are shown to scale as well as the discriminator level. The bulk of the recorded events lies between the extreme cases for protons and mesons, between a and b and between c and d respectively.

At H.V. (1) all pulses are too small to be accepted and the counting rate is zero, as shown in the bottom diagram of Figure 6, but the largest pulse, a is at exactly the discriminator level.

At H.V. (2) the pulses have been amplified enough so that about half of all the proton pulses have heights greater than the discriminator level and are counted.

At H.V. (3) all the pulses due to protons are above the discrimination level and are counted. The pulses due to the mesons are below the discrimination level and thus are not counted. Until the voltage is raised enough for the meson pulses to be greater than the discrimination level, the counting rate will remain constant.

At H.V. (4) we accept the largest meson pulse and at H.V. (5) we accept the smallest meson pulse and are counting all the mesons.

At H.V. (6) the counting rate is the same as we are counting all the particles at H.V. (5).

The regions 3-4, 5-6 we call plateaus for in these regions a change in H.V. does not affect the counting rate and within these regions we discriminate against particles of different mass. In particular, in region 3-4, we discriminate against mesons. If we wished to know the number of mesons we would subtract the height of plateau 3-4 from the height of plateau 5-6. The width of plateau 3-4, W_1, depends upon the merit ratio $\Delta E_b/\Delta E_c$, the proportionality of the counter system, and the voltage-gain characteristics of the photomultiplier tubes used.

E. Experimental Coincidence Plateau

The preceding ideal counting rate plateaus were not to be expected in practice for several reasons. There were deuterons and electrons from the carbon target which was bombarded for calibration purposes. The deuterons and electrons tend to smear out the proton plateau at the low end and the meson plateau at the high end respectively. In addition one has statistical fluctuations in the counting rates at different high voltages. A counting rate/unit beam vs. counter No. 1 photomultiplier

high voltage curve is shown in Figure 7. The counting rate figures are the actual experimental results and an inspection of the numbers shows one what order of statistical fluctuation to expect. The solid curve is the experimental equivalent of the ideal coincidence plateau.

F. Chi^2 Test

Having an experimental counting rate vs. Counter No. 1 high voltage curve, one can try to fit the data with the ideal coincidence plateau developed in D. One uses the experimental data to fix the voltage points which actually correspond to (1), (2), (3).....in that treatment. Since the actual counting rate during calibration was low the statistical fluctuations in the data would be expected to make some points lie off the "plateau" by several standard deviations. If one actually had no power to discriminate one particle from another one might expect a smooth increase in counting rate as the photomultiplier high voltage was raised. The best straight line through these points would, therefore, be a good alternative to the plateau type of curve. The best straight line is the one which yields the smallest Chi^2 (χ^2) with the experimental data. By χ^2 we mean the square of the difference between the experimental point and the point on our hypothetical curve divided by the value of our hypothetical curve summed over the number of experimental points we have, i.e., $\sum_i \frac{(Y_i-Z_i)^2}{Z_i}$ where Y_i is the experimental value and Z_i is the value that lies on our hypothetical curve. The χ^2 was also determined for the plateau type curve. In order to compare the relative χ^2's one must use a χ^2 table, since the two curves have a different number of degrees of freedom in the statistical sense.

The language used expresses the excellence of a hypothetical curve's fit to a certain group of data by the probability of any other group of experimental data's χ^2 being larger than the χ^2_p of our particular group of data. If our χ^2_p is small, our curve is a good fit to the data, and we would expect this probability to be large. However if our χ^2_p is large indicating a bad fit to the data, we would expect this probability to be small. For the counting rates we had and the number of points (high voltage) we took we have the following probabilities:

$$\text{plateau curve } P\ (\chi^2)_{pl} \geq (\chi^2)_{exp_{pl}} = 80 \text{ percent}$$

$$\text{straight line } P\ (\chi^2_{st}) \geq (\chi^2_{exp_{st}} = 50 \text{ percent}$$

It must be reemphasized that the $(\chi^2)_{pl}$ are not equal to $(\chi^2)_{st}$ because the two hypothetical curves with which the experimental data is compared, are different.

In order to differentiate between two hypothetical curves which might seem to fit the experimental data, we must do two things. We must show that one of the hypothetical curves, the one we choose, has a high probability of being the curve which truly represents the experimental data. We must also show that the alternative hypothetical curve has a very low probability of truly representing the experimental data. It is not enough to show that one curve has a high probability of fitting the data without having good criteria for rejection of alternative curves. We can see this borne out by the probability figures above.

Although the probability of the plateau's being the true curve is slightly higher (80 percent compared with 50 percent), the test as here applied is inconclusive. The reason for this is that we have no power of rejection of the false hypothesis, which we assume the straight line to be. The primary reason is that the individual counting points do not contain large enough numbers to differentiate two curves that are everywhere so close together. The use of the non-central χ^2 test as developed by Bayard Rankin[10] indicates that it would be necessary to run 4 - 10 times as long in calibration in order to make the test conclusive, i.e.,

$$\text{plateau curve} \quad P\,(\chi^2)_{\text{plateau}} \geq (\chi^2_{\text{exp}})_{\text{plateau}} > 50 \text{ percent}$$

$$\text{straight line} \quad P\,(\chi^2)_{\text{S. L.}} \geq (\chi^2_{\text{exp}})_{\text{S. L.}} < 3 \text{ percent}$$

Such probabilities would enable us to reject the false hypothesis, which we assume the straight line to be.

Since over a third of the entire machine time devoted to this experiment was used for obtaining the data that appears on the plateau curve calibration, running 4 to 10 times as long is not practical at this particular time. In the future, however, the use of the χ^2 test offers a conclusive test of the validity of the plateau type curve. Other proofs were obtained of the discrimination of the telescope system.

G. Cyclotron Run

90 Mev neutrons from the stripped deuteron beam of the 184-in. synchro-cyclotron were used to bombard a paraffin target. No mesons could be produced at this bombardment energy and thus the only particles that could enter the telescope system were protons and heavier particles. The

counting rate vs. photomultiplier high voltage is shown in Figure 8. It can be seen that a fairly good plateau was obtained. The collimation was not quite as good as it was at the synchrotron and this is one of the reasons that the plateau is not sharper. The proton operating point was taken to be 1400 volts and from this particular curve, this point might be one at which the system differed from an efficiency of 100 percent by as much as 10 percent. However, the statistics are such that any correction could not be exact and thus the assumption of 100 percent efficiency was made.

H. Protons and Mesons from Carbon

Another test for the system is to count the protons and mesons from the photon bombardment of carbon at 90° to the beam. The meson cross sections can be compared with the work of Peterson, Gilbert, and White[11]. The proton cross sections can be compared with other work [12,13] which, although not consistent, is indicative of what one might expect.

The 3/4 inch thick carbon target 45° to the beam and 45° to the telescopes was the one used for the counting rate vs. photomultiplier high voltage calibration. Various thicknesses of absorber were used and for each thickness two separate runs were made, one with the photomultiplier high voltage on the "proton" plateau and the other on the "meson" plateau. The "proton" plateau actually included protons and all heavier particles, and the "meson" plateau included mesons and protons and all heavier particles. To find the number of mesons, one subtracted the "proton" counting rate from the "meson" counting rate.

There were two independent telescope systems and in Figures 9, 10 are shown the "proton" cross sections vs. proton energy for both of them.

In Figures 9, 10 the curves are shown corrected for nuclear absorption with dotted lines. The running times for this series of calibrations were, of necessity, short and thus the standard deviations on individual points are large. However, they are small enough for us to determine the character of these curves and those for meson production so as to allow little doubt that the operating conditions were, in fact, correct. The energy resolution for the systems was not good because a thick target was used to maximize the counting rate. We can conclude that our cross section for proton production is in fair agreement with that of Keck[13] and the dependence of the cross section with energy of the emitted proton is in fair agreement with that Silverman and Levinthal found at lower proton energies[12].

In Figure 11 is shown the meson cross sections determined in this calibration. The solid curve is that of Peterson, Gilbert, and White[11]. Within the statistics of the measurements the agreement must be considered satisfactory.

I. Summary

The machine time required to obtain enough counts to make any one of the calibration methods conclusive is prohibitive. However, taking the various calibration procedures, each of which shows a large probability that the operating conditions were proper, as a whole, we feel that there is an overwhelming probability that at the operating conditions at which the experiment was run, protons were counted with at least 90 percent efficiency and no mesons were detected. In addition, when one used the equipment to count mesons, one could detect them with close to 100 percent efficiency.

V EXPERIMENTAL PROCEDURE

Once the calibration with the carbon target had been completed, the deuterium pressure target was put in place and aligned as described in Section III.

A. E_γ by (E_p, θ_p)

$\gamma + D \rightarrow p + n$ represents a two body problem both before the photon interaction and afterward. At high γ energies it is possible for mesons to be produced as well as two nucleons but in such cases, because approximately 140 Mev of energy are required to create the meson as well as the kinematics of the conservation of momentum between the meson and any recoil nucleons, the energy of an emerging proton would be below the threshold of our detection system (90 Mev at 90^o). Therefore all the protons observed are due to the reaction above. The equations used are developed in the Appendix, IX.

B. Beam Monitor

To monitor the beam, three ionization chambers, two in front of the target and one in back of the target, were used simultaneously. Their ratios remained constant throughout the experiment. The absolute calibration was based on the method of Blocker, Kenney, and Panofsky[14, 15].

They estimate the absolute calibration to be accurate to within 20 percent. All the cross sections, therefore, are to be understood to be quoted in the absolute sense to within 20 percent. This is above and beyond the quoted uncertainties which are primarily statistical. However any uncertainty in the absolute calibration would not change the relative

experimentally determined cross sections as the ionization chambers did not drift during the course of the experiment, as is evidenced by the fact that the ratios among the three chambers remained constant.

VI ANALYSIS OF DATA

A. Determination of Geometrical Factor

The deuterium target can be considered as a line source viewed by a two slit collimator system, both slits of which are circular and are of the same size. In order to determine the effective solid angle subtended by the collimation system to the line target, the following construction was used.

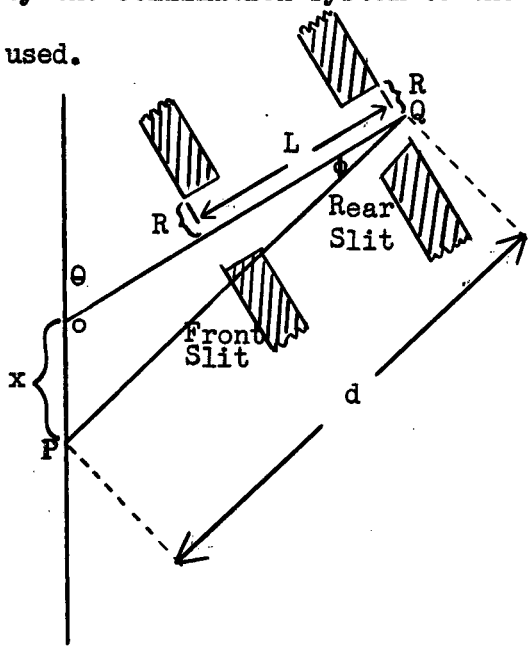

$a = OQ$

$d = PQ$

$d^2 = a^2 + x^2 + 2ax \cos \theta$

$\sin \phi = \frac{x \sin \theta}{d}$

Ω_{rear} from P $= \frac{\pi R^2}{d^2}$ steradians

To point P on the target, the near circular slit subtends a large solid angle than does the rear circular slit, and therefore the near slit looks larger.

The apparent ratio in order to project both slits to a common point is $R = \frac{d}{d - \frac{L}{\cos \phi}}$ i.e., draw the rear circular slit with R = R actual,

the front circular slit with $R' = R$ actual $\frac{d}{d - \frac{L}{\cos \phi}}$.

The centers of the two circles should be separated by $\frac{d}{d - \frac{L}{\cos \phi}}$ L sin ϕ.

The reason for the factor $\frac{d}{d - \frac{L}{\cos \phi}}$ entering both the apparent radius of the front slit and the apparent translation of this slit relative to the rear one is that, in this treatment, both front and rear slits are projected to be at point P on the line target and this factor is required in order to make the projection a true one. Using this projection one can obtain an "effective solid angle" subtended at the target element by the collimator system. This "effective solid angle" is equal to the solid angle subtended by the rear collimator slit times f, where f is the factor relating to what fraction of the counter hole can be seen from P.

Example: Rear hole from P has apparent area A.

The front slit partially obscures rear slit

$$f = \frac{O \text{ (area of overlap)}}{A}$$

Using this method, one can determine the effective solid angle the collimation system subtends to the line target for all x, the distance from the center of the target.

$\int$"Ωeff" dx can then be determined and is used in the calculations of the cross sections.

B. Bremsstrahlung Curve Corrected for "Spread Out" Beam

The theoretical bremsstrahlung curve for 324 Mev electrons, which correspond to the peak energy, striking a 0.020 inch platinum target is shown as A in Figure 12. In the "spread out" beam, however, the electrons are of various energies corresponding to the magnetic field at the time they strike the synchrotron target. Figure 13 is a picture of the beam which shows the relative intensity vs time of the emergent beam. The timing markers are 1000 μsec apart. The energy of the electrons = $324 \sin\left(\frac{7790 - x}{7790}\right) 90^\circ$ where x is the time in μsec from the peak field at which the electrons strike the platinum target.

Equivalent bremsstrahlung spectra corresponding to the various quantum limits (electron energies) were drawn and added using the relative beam intensities as the weighting factors. The resultant curve is shown as B in Figure 12.

C. Cross Section Determination

$$\left(\frac{\text{no. counts}}{\text{unit beam}}\right)_{\theta,E_\gamma} C = \left(\frac{d\sigma(E_\gamma)}{d\Omega}\right)_\theta \frac{x\ \Delta E_\gamma}{\Delta E_p} x\ \Delta E_p \cdot \frac{\text{No photons of energy } E_\gamma}{\text{Unit beam unit } \Delta E_\gamma} x \frac{\text{no. atoms}}{cm^3} x \int \text{"}\Omega\text{eff" dx}$$

$$\text{or } \left(\frac{d\sigma(E_\gamma)}{d\Omega}\right)_\theta = \left(\frac{\text{no. counts}}{\text{unit beam}}\right)_{\theta,E_\gamma} C \Big/ \Delta E_p \ x \frac{\Delta E_\gamma}{\Delta E_p} \ x \frac{\text{no. photons}}{\text{unit beam unit } \Delta E_\gamma} x \frac{\text{no atoms}}{cm^3} \cdot \int \text{"}\Omega\text{eff" dx}$$

where $\left(\frac{d\sigma(E_\gamma)}{d\Omega}\right)_\theta$ is the differential cross section in cm^2/steradian photon for a photon energy = E_γ

$\frac{\Delta E_\gamma}{\Delta E_p}$ is the ratio of the spread in γ-energy corresponding to the spread in proton energy ΔE_p, or energy bite, selected by the counter system.

$\frac{\text{No. photons}}{\text{unit beam unit } \Delta E_\gamma}$ = no. of photons of energy E_γ in a 1 Mev interval per unit beam (Using curve of VI B).

$\frac{\text{No. atoms}}{cm^3}$ = density of deuterium at 2000 P.S.I. and 77° K = 2.52×10^{22} atoms/cm^2

$\int$"Ωeff"dx = Length of line target contributing to counting rate times average solid angle (see Section VI A.)

C = correction term (see VI D).

In order to transform to center of mass system, one uses (see Appendix)

$$\frac{d\Omega_{c.m.}}{d\Omega_{lab}} = \gamma \frac{\sin^3\theta'}{\sin^3\theta}\left(1-\frac{\beta E_p}{\sqrt{E_p^2-Eo_p^2}}\cos\theta\right)$$

$$\left(\frac{d\sigma(E_\gamma)}{d\Omega_{c.m.}}\right)_{\theta'_{c.m.}} = \left(\frac{d\sigma(E_\gamma)}{d\Omega_{lab}}\right)_\theta \Big/ \gamma\frac{\sin^3\theta'}{\sin^3\theta}\left(1-\frac{\beta E_p}{\sqrt{E_p^2-Eo_p^2}}\cos\theta\right)$$

the total cross section

$$\sigma_t(E_\gamma) = \int\left(\frac{d\sigma(E_\gamma)}{d\Omega_{lab}}\right)_\theta d\Omega = 2\pi\int\left(\frac{d\sigma(E_\gamma)}{d\Omega_{lab}}\right)_\theta \sin\theta\, d\theta$$

$$\text{or } \sigma_t(E_\gamma) = 2\pi\int\left(\frac{d\sigma(E_\gamma)}{d\Omega_{c.m.}}\right)_{\theta'} \sin\theta'\, d\theta'$$

D. Corrections

1. Nuclear Interaction in Absorbers and the Target Walls

The protons in traversing matter may interact with the nuclei. They may be absorbed or undergo large angle scattering, in either case not reaching the detector. The cross section was taken to be of the order of a geometrical nuclear area[9]. The radius was taken to be $1.4 \times 10^{-13} A^{1/3}$ cm, and for copper this yielded a mean free path $\lambda = 111$ grams/cm^2. Wherever the correction has been made, it has been indicated by a dotted line unless otherwise specified. The resultant correction factors are shown in Fig. 14 and in practice ranged up to a 40 percent correction.

2. Multiple Scattering

Due to small angle multiple scattering some protons that are initially directed toward the detection system have their directions altered in traversing the absorbers and strike the rear collimator, thereby not reaching the detector. The normal curve $P = \frac{1}{\sqrt{2\pi}} e^{-\theta^2/2\bar{\theta}^2}$ was used for the distribution function and approximate formula $\overline{\theta^2} = \frac{E_s^2}{p^2\beta^2} t$ was used where $E_s = 21$ Mev, t = thickness of absorbers in radiation lengths, (22.4 gm). This function was then numerically integrated for various points on the detector for various absorber thicknesses. The resultant correction factors for the data are shown in Fig. 15. In practice, the maximum correction due to this cause was 31 percent.

3. Slit Penetration

The geometrical factors were calculated on the basis of slots perfectly opaque to the protons. The final slit was of lead and the range

energy relationship for protons is such, combined with the required path length through the lead necessary to increase the solid angle perceptibly, that the effect of penetration is negligible.

4. Efficiency of Detectors

It has been pointed out in IV G. that one might conclude the operating point was one for which the efficiency for the detection of protons was 95 ± 5 percent. The efficiency of 100 percent is used since no correction term of any precision is known.

VII RESULTS

A. Differential Cross Sections

The angular resolution is such that the bulk of the particles counted were emitted at $\theta \pm 4^{\circ}$. However a few particles are from the angular range from 4°-6° from θ. Therefore all the particles are emitted with $\theta \pm 6^{\circ}$. There is an energy uncertainty in the bombarding γ-ray due to this angular uncertainty. This uncertainty is smallest for small θ and increases with θ. For $\theta = 30^{\circ}$, ΔE_{γ} due to this cause is about 6 Mev. For $\theta = 90^{\circ}$, $\Delta E_{\gamma} = 12$ Mev.

The energy uncertainty due to the thickness of the second counter varies from about 7 Mev at 30° to about 15 Mev at 90 degrees. Thus there is a different energy uncertainty for every angle but we can approximate these uncertainties by assigning an overall uncertainty to the bombarding γ-rays of 15 Mev., i.e., the two energy bands of bombarding photons were 200 ± 15 Mev, and 250 ± 15 Mev, both in the center of mass system. These correspond to γ-ray energies of 233 and 286 Mev respectively in the laboratory system.

The $\left(\frac{d\sigma(E_{\gamma})}{d\Omega\,\text{lab}}\right)_{\theta\text{lab.}}$ vs θ_{lab} are plotted for 200 ± 15 Mev (C.M.) and 250 ± 15 Mev (C.M.) in Fig. 16 and Fig. 17 respectively.

The $\left(\frac{d\sigma(E_{\gamma})}{d\Omega\,\text{c.m.}}\right)_{\theta_{\text{C.M.}}}$ vs $\theta_{\text{C.M.}}$ for 200 and 250 Mev are shown in Fig. 18 and Fig. 19 respectively.

When the deuterium gas was pumped out of the target in order to determine the background counting rate due to the target assembly, it was discovered that this no - gas counting rate was unexpectedly large. Although the target assembly was aligned with the beam by photographic means, it is felt that perhaps the secondary collimator was slightly misaligned and was struck by the fringe of the photon beam. In any case the no - gas counting rate at some angles was as large as a third of the deuterium counting rate. Singularly it was found that one of the two telescopes recorded more background than the other, probably because the fringe beam was striking one side of the target assembly. The subtraction of this background was such that statistically there was no point in trying to combine the data of the two telescopes. Therefore the data was taken from the telescope which had the smaller background or no - gas counting rate. The only point for which the other telescope was used was the 30° point which only it could reach. Within the statistics the cross sections from the telescope whose data was not used, agree with those that appear here.

B. Total Cross Sections

The total cross section $\sigma_t(E_\gamma) = 2\pi \int \left(\frac{d\sigma(E_\gamma)}{d\Omega_{C.M.}}\right)_{\theta'_{C.M.}} \sin \theta_{C.M.}$

$d\theta_{C.M.}$ was found by performing the integration graphically. In addition to the uncertainties listed previously, there is the uncertainty due to the extrapolation over angles for which the differential cross sections were not obtained. Since the solid angle approaches zero at 0° and 180°, and since the differential cross sections apparently drop at large and small angles, the error due to this extrapolation is minimized.

The total cross sections are given in Table I.

Energy E_γ(C.M.)	σ_t in $\frac{cm^2}{photon}$	σ_t corrected for nuclear absorption
200 ± 15	$(8.1 \pm 2.4)\times10^{-29}$	$(10.0 \pm 3.0)\times10^{-29}$
250 ± 15	$(12.9 \pm 5.2)\times10^{-29}$	$(15.9 \pm 6.4)\times10^{-29}$

The absolute beam calibration is quoted to 20 percent. Therefore these absolute cross sections could vary by an additional 20 percent for this reason.

VIII CONCLUSIONS

The total cross sections to be expected in the photon energy range 150-250 Mev have been calculated [6,7,8], not taking into account meson interactions. Two of these calculations[7,8] are carried out up to about 150 Mev and the other[6] is carried out as far as 300 Mev. The character of all of these predicted cross sections is the same, viz., the σ_t decreases as the energy increases and at 150 Mev is about 1.5 x 10^{-29} cm^2/photon. In Figures 20, 21, 22 are shown the three different calculated cross section dependence on γ-energy with our experimental data superimposed.

The observed σ_t (200 ± 15) = (10.0 ± 3.0)x10^{-29} cm^2/photon is incompatible with a σ_t (150) = 1.5-2 x 10^{-29} cm^2/photons and decreasing with energy or even remaining constant. Since the theoretically derived cross sections used parameters based on other experiments, primarily n-p scattering, one might expect that the calculations should be good for energies corresponding to these other experiments. That is photodisintegration at 150 Mev γ-energy involves the same n-p forces as approximately 300 Mev n-p scattering experiments. The only way the meson contributions were used in the calculations was in the assumption of 50-50 exchange-ordinary force.

The data for σ_t(250 ± 15 Mev) compared with σ_t (200 ± 15 Mev) indicates that above 140 Mev the cross section increases with energy. If one extrapolates the σ_t vs. E_γ curve to 140 Mev using our σ_t (200) and σ_t (250), the σ_t (140) is still much larger than the theoretically

derived cross sections mentioned above. The statistical nature of the data for σ_t (200) and σ_t (250) is such that although it seems that σ_t rises from 200 Mev to 250 Mev, one cannot, on statistical grounds, preclude the possibility that σ_t may remain constant or even fall slightly between 200 and 250 Mev. Therefore the extrapolation to 140 Mev cannot be made with any precision. It should be emphasized that the σ_t being considered is for the $\gamma + D \rightarrow p + n$ reaction only and, energetically, reactions in which mesons are ejected do not enter into our measurements.

One concludes therefore that above the meson threshold, 140 Mev, the cross section rises with energy. Also the cross section of deuteron photodisintegration is much larger at 140 Mev than theories ignoring meson contributions can explain.

One possibility might be that the real meson which is produced by the $\gamma + D \rightarrow \pi + 2$ nucleons reaction might be reabsorbed. If such a meson is reabsorbed, the overall kinematics are those of the two-body problem i.e., only those γ-energies which correspond to the emitted proton's energy and angle of emission are effective. Only the mesons produced by this narrow band of γ-energies can be effective. The number of such mesons is so small that even if all the real mesons produced from deuterium (see 9) were reabsorbed (which they are not), their number would still be too small to explain the observed cross sections. Further proof is given by the angular dependence of the differential cross sections (Figures 18 and 19) which are both peaked sharply forward. If meson reabsorption was significant, one would expect a distribution either isotropic or peaked slightly backwards, as is the meson distribution. From both these considerations,

one concludes that the reabsorption of real mesons is not a significant factor and cannot explain the observed results.

On the other hand, the role virtual mesons play is not negligible. One might consider the electromagnetic field of the incident photon as being coupled to the exchange currents caused by the virtual mesons. Such an interaction is not obvious nor easy to visualize in a qualitative way. However preliminary theoretical calculations made by Huddlestone and Lepore[16] indicate that the cross section one would expect from this coupling with the exchange current is of the same order of magnitude as the observed results. It is still much too early to claim that agreement has been reached in any sort of a quantitative manner.

IX APPENDIX

The kinematical relationships used were derived using the Lorentz transformations. Consider the γ + D kinematics:

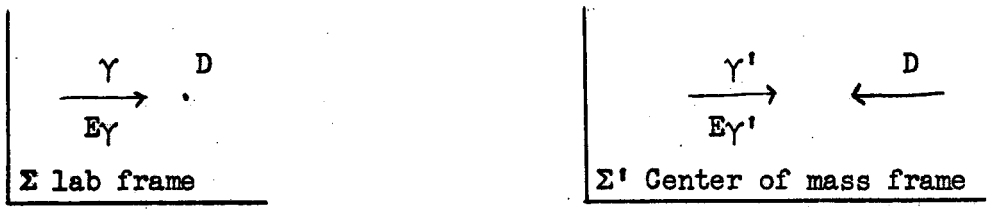

β is relative velocity of frames

$$\left(4 \text{ vector } \chi\right) = \begin{pmatrix} \gamma & 1 & \beta\gamma \\ \beta\gamma & 1 & \gamma \end{pmatrix} \qquad (\chi')$$

For γ $\quad E_\gamma = \beta\gamma cp' + \gamma E_\gamma'$

but for γ rays, $cp_x' = E_\gamma'$

$\therefore E_\gamma = \gamma (1 + \beta) E_\gamma'$ $\qquad$ E_γ' = energy of γ in center of mass

E_γ = energy of γ in lab

For γ + D system

$p' = 0$ by definition

$cp = E_\gamma$

$E = E_\gamma + E_{oD}$ where E_{oD} = rest energy of deuteron

Using transformations $\quad cp = \beta \gamma E'$

$E = \gamma E'$

but $cp = E_\gamma$

$E = E_\gamma + E_{oD}$ $\qquad$ $\beta = \dfrac{E_\gamma}{E_\gamma + E_{oD}}$

Consider the emergent protons

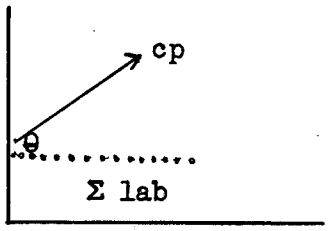

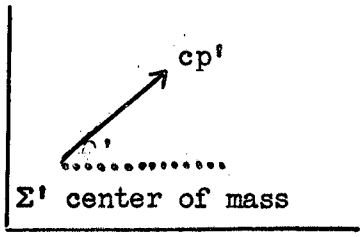

$$cp_x = \gamma\, cp_x' + \beta\gamma E_p'$$

$$E_p = \beta\,\gamma\, cp_x' + \gamma\, E_p'$$

$$cp_y = cp_y'$$

$$cp\cos\theta = \gamma\, cp'\cos\theta' + \beta\,\gamma\, E_p'$$

$$cp\sin\theta = cp'\sin\theta'$$

$$E_p = \beta\,\gamma\, cp'\cos\theta' + \gamma\, E_p'$$

but $cp'_{proton} = \sqrt{E_p'^2 - Eo_p^2}$

$$\therefore E_p = \beta\,\gamma\cos\theta' \sqrt{E_p'^2 - Eo_p^2} + \gamma\, E_p'$$

$$E' = \frac{E_\gamma + Eo_D}{\gamma} = E_p' + E_n' \cong 2E_p' \qquad \text{where } \gamma = \frac{1}{\sqrt{1-B^2}}$$

$$E_p' = \frac{E_\gamma + Eo_D}{2\gamma} = 1/2 \sqrt{2\, E_\gamma Eo_D + Eo_D^2}$$

Now $Eo_D = E_{o_p} + E_{o_n}$ - (Binding) $= 2\, E_{o_p} - B + (E_{o_n} - E_{o_p})$

$\sim$ 1.3 Mev

$$Eo_D = E_{o_p} - b \text{ where } b = B - 1.3 \cong 1 \text{ Mev}$$

Also $T_p = E_p - E_{o_p}$

$$\therefore\ T_p = \frac{E_\gamma - b}{2} + \frac{E_\gamma}{2}\cos\theta' \sqrt{\frac{E_\gamma}{E_\gamma + Eo_p}}$$

Transformations of angles and solid angles

Since we measure our angles and solid angles in the laboratory system, we are interested in the transformations to the center of mass system.

$$(\chi') = \begin{pmatrix} \gamma & -\beta\gamma \\ -\beta\gamma & \gamma \end{pmatrix} (\chi)$$

$$\tan\theta' = \frac{p'_y}{p_x} = \frac{c\,p_y}{c\,\gamma\,p_x - \beta\,\gamma\,E_p} = \frac{\frac{1}{\gamma\frac{p_x}{p_y} - \frac{\beta\,\gamma\,E_p}{cp_y}}}{}$$

$$\tan\theta' = \frac{1}{\gamma\cot\theta - \frac{\beta\,\gamma\,E_p}{\sqrt{E_p^2 - E_{o_p}^2\sin\theta}}}$$

$$\cot\theta' = \gamma\cot\theta - \frac{\beta\,\gamma\,E_p}{\sqrt{E_p^2 - E_{o_p}^2\sin\theta}}$$

after differentiation

$$-\csc^2\theta'\,d\theta' = -\gamma\csc^2\theta\,d\theta + \frac{\beta\,\gamma\,E_p}{\sqrt{E_p^2 - E_{o_p}^2}}\cot\theta\csc\theta\,d\theta$$

$$d\theta' = d\theta\;\gamma\;\frac{\sin^2\theta'}{\sin^2\theta}\left(1 - \frac{\beta\,E_p}{\sqrt{E_p^2 - E_{o_p}^2}}\cos\theta\right)$$

$$\frac{d\Omega'}{d\Omega} = \frac{2\pi\sin\theta'\,d\theta'}{2\pi\sin\theta\,d\theta} = \gamma\,\frac{\sin^3\theta'}{\sin^3\theta}\left(1 - \frac{\beta\,E_p}{\sqrt{E_p^2 - E_{o_p}^2}}\cos\theta\right)$$

X ACKNOWLEDGMENTS

It is a pleasure to acknowledge the continued guidance and support of Professor A. C. Helmholz. I am indebted to Mr. J. W. Rose for his cooperation throughout the course of the experiment; and thanks are due Dr. R. S. White for the use of his high pressure deuterium target assembly and his assistance in the use of both it and the deuterium pumping system, and to Mr. John Barale of the Electronics Group for the development of the pulse height discriminator circuits and for maintenance of the electronics used. My sincere thanks go to Mr. George McFarland and the entire synchrotron crew for their cooperation in making the bombardments.

XI REFERENCES

1. Bethe and Peierls, Proc. Roy. Soc. A148, 146 (1935)
2. Fermi, Phys. Rev. 48, 570 (1935)
3. Bethe and Bacher, Rev. Mod. Phys. 8 (1936)
4. Fuller, Phys. Rev. 79, 303 (1950)
5. Wilkinson and Carver, Nature 167, 154-5
6. Marshall and Guth, Phys. Rev. 76, 1880 (1949)
7. Schiff, Phys. Rev. 78, 734 (1950)
8. Marshall and Guth, Phys. Rev. 78, 739 (1950)
9. R. S. White, Ph.D. Thesis, University of California, UCRL-1319
10. B. Rankin, Private communication, UCRL
11. Peterson, Gilbert and White, Phys. Rev. 81, 1003-1011 (1951)
12. Levinthal and Silverman, Phys. Rev. 82, 822 (1951)
13. Levinger, Phys. Rev. 84, 51 (1951)
14. Blocker, Kenney, and Panofsky, Phys. Rev. 79, 419 (1950)
15. McMillan, Blocker and Kenney, Phys. Rev. 81, 455 (1951)
16. Huddlestone and Lepore, private communication, UCRL

XII ILLUSTRATIONS

Fig. 1 - Schematic arrangement of the apparatus with respect to the synchrotron.

Fig. 2 - Assembly of the gas target.

Fig. 3 - Schematic drawing of the high pressure system.

Fig. 4 - Photograph of the target, counter houses, and collimator assembly, looking from the synchrotron.

Fig. 5 - Photograph of target and counting assembly, looking toward the synchrotron.

Fig. 6 - Ideal coincidence plateau diagram.

Fig. 7 - Experimental plateau (at synchrotron).

Fig. 8 - Experimental plateau (at cyclotron).

Fig. 9 - Proton $\left(\frac{d\sigma}{d\Omega}\right)$ at 90° vs. E_p from carbon - telescope 1.

Fig. 10 - Proton $\left(\frac{d\sigma}{d\Omega}\right)$ at 90° vs. E_p from carbon - telescope 2.

Fig. 11 - Meson cross sections from carbon at 90°. Solid curve is from Ref. 11.

Fig. 12 - Bremsstrahlung curve.

Fig. 13 - Picture of beam.

Fig. 14 - Correction for nuclear absorption.

Fig. 15 - Correction for multiple scattering.

Fig. 16 - $\left(\frac{d\sigma}{d\Omega}\right)_\theta$ vs. θ for deuterium. E_γ = 200 Mev lab system.

Fig. 17 - $\left(\frac{d\sigma}{d\Omega}\right)_\theta$ vs. θ for deuterium. E_γ = 250 Mev lab system.

Fig. 18 - $\left(\frac{d\sigma}{d\Omega}\right)_\theta$ vs. θ for deuterium. E_γ = 200 Mev center of mass system.

Fig. 19 - $\left(\frac{d\sigma}{d\Omega}\right)_\theta$ vs. θ for deuterium. E_γ = 250 Mev center of mass system.

Fig. 20 - Comparison of experimental σ_t with theory. Solid curve from Ref. 6.

Fig. 21 - Comparison of experimental σ_t with theory. Solid curve from Ref. 7.

Fig. 22 - Comparison of experimental σ_t with theory. Solid curve from Ref. 8.

Fig. 23 - Block diagram of electronics.

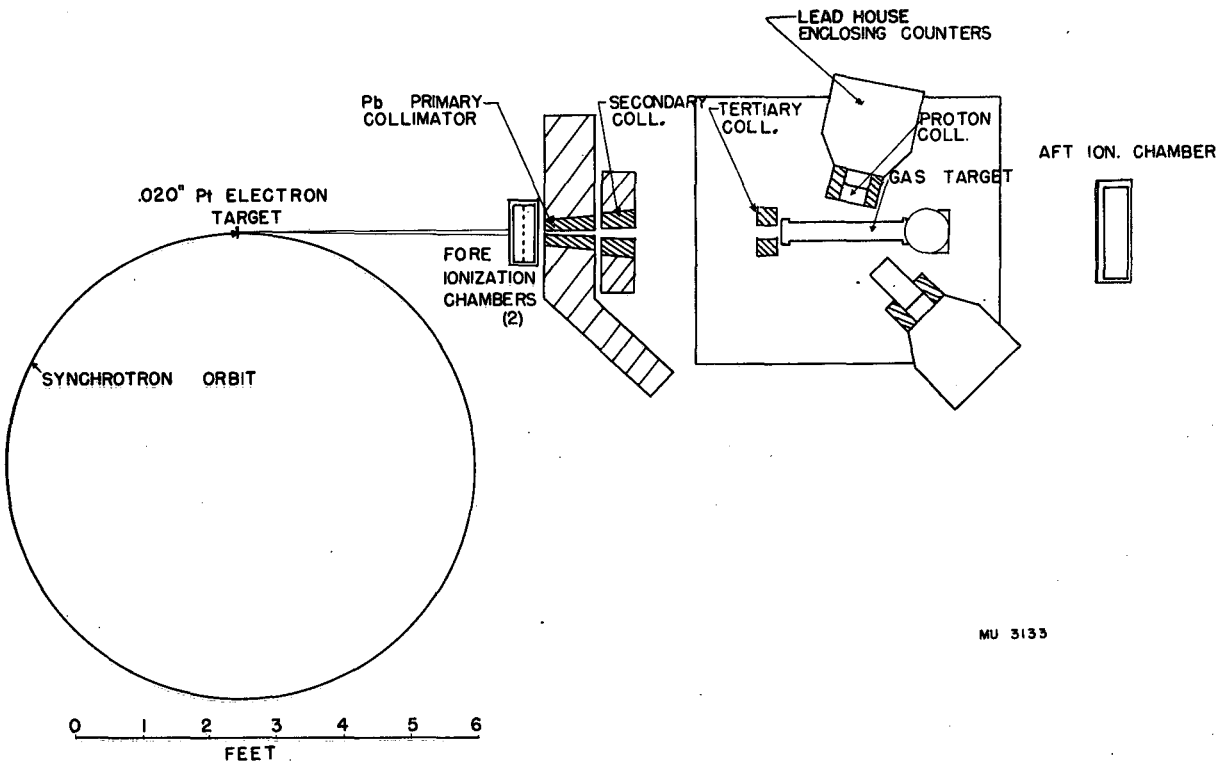
LEAD HOUSE
ENCLOSING COUNTERS
Pb PRIMARY
COLLIMATOR
SECONDARY
COLL.
TERTIARY
COLL.
PROTON
COLL.
AFT ION. CHAMBER
GAS TARGET
.020" Pt ELECTRON
TARGET
FORE
IONIZATION
CHAMBERS
(2)
SYNCHROTRON ORBIT
MU 3133
0 1 2 3 4 5 6
FEET

Fig. 1

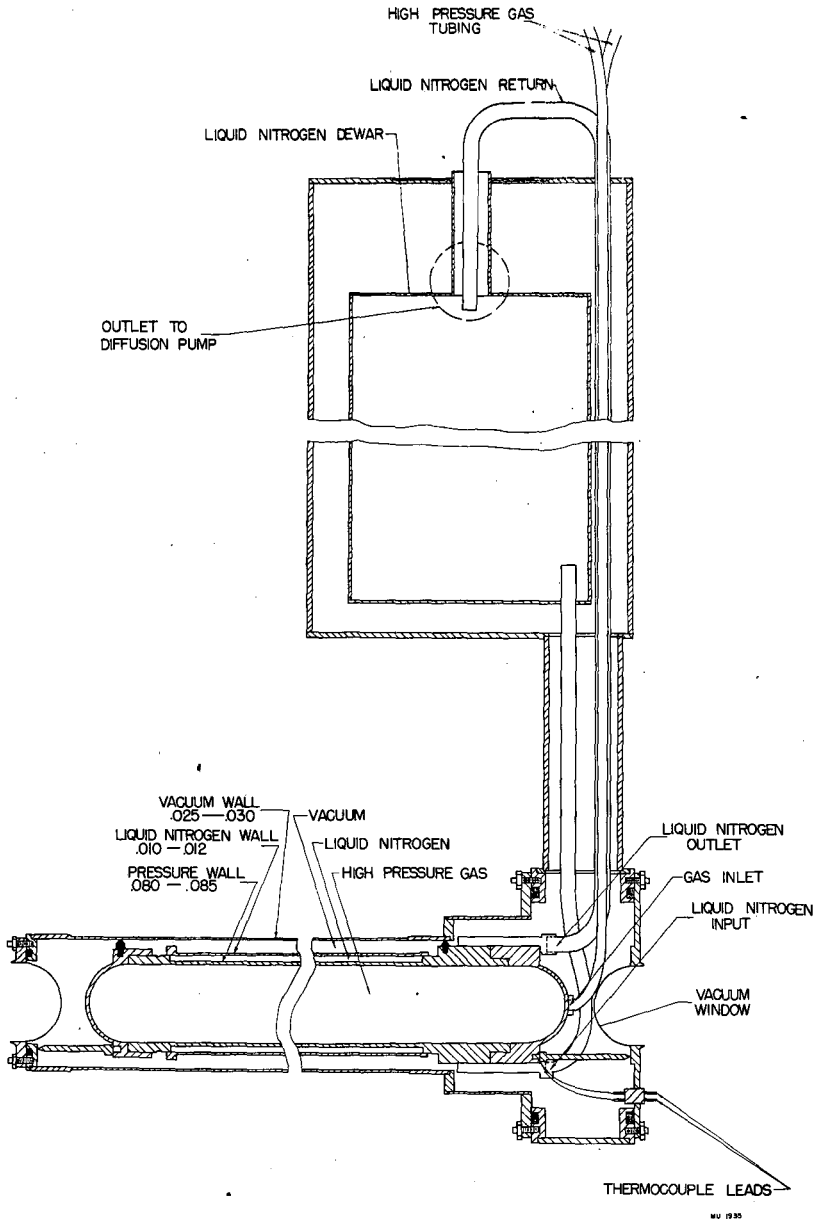
HIGH PRESSURE GAS TUBING
LIQUID NITROGEN RETURN
LIQUID NITROGEN DEWAR
OUTLET TO DIFFUSION PUMP
VACUUM WALL .025 — .030
LIQUID NITROGEN WALL .010 — .012
PRESSURE WALL .080 — .085
VACUUM
LIQUID NITROGEN
HIGH PRESSURE GAS
LIQUID NITROGEN OUTLET
GAS INLET
LIQUID NITROGEN INPUT
VACUUM WINDOW
THERMOCOUPLE LEADS

Fig. 2

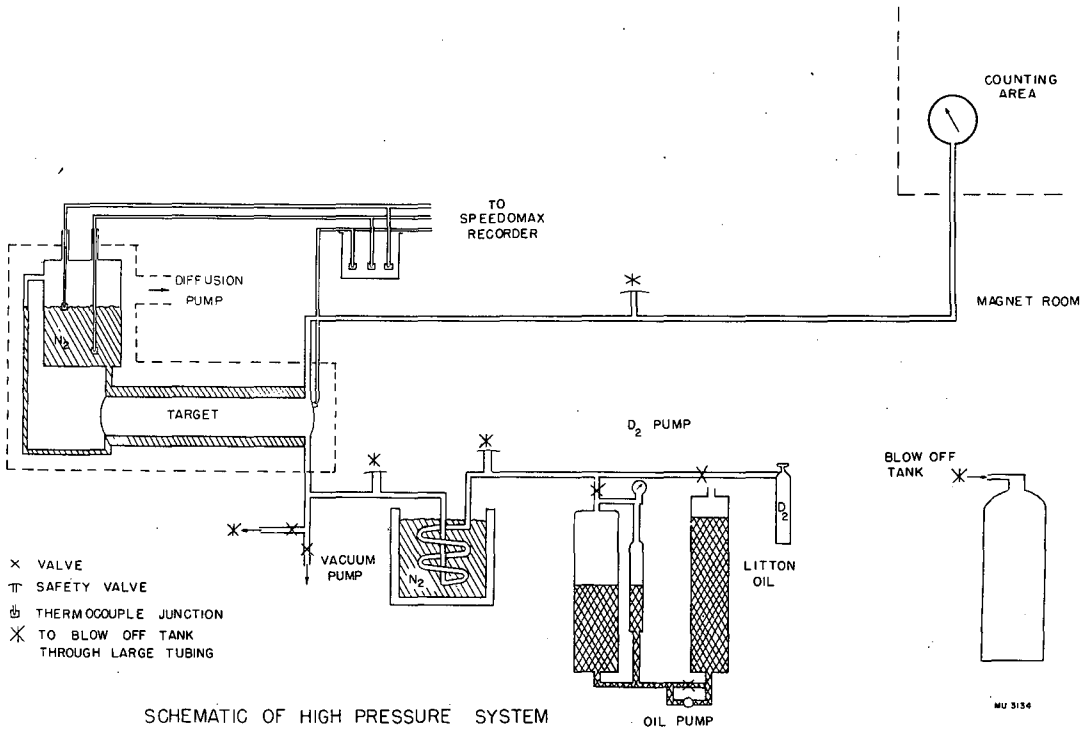

SCHEMATIC OF HIGH PRESSURE SYSTEM

Fig. 3

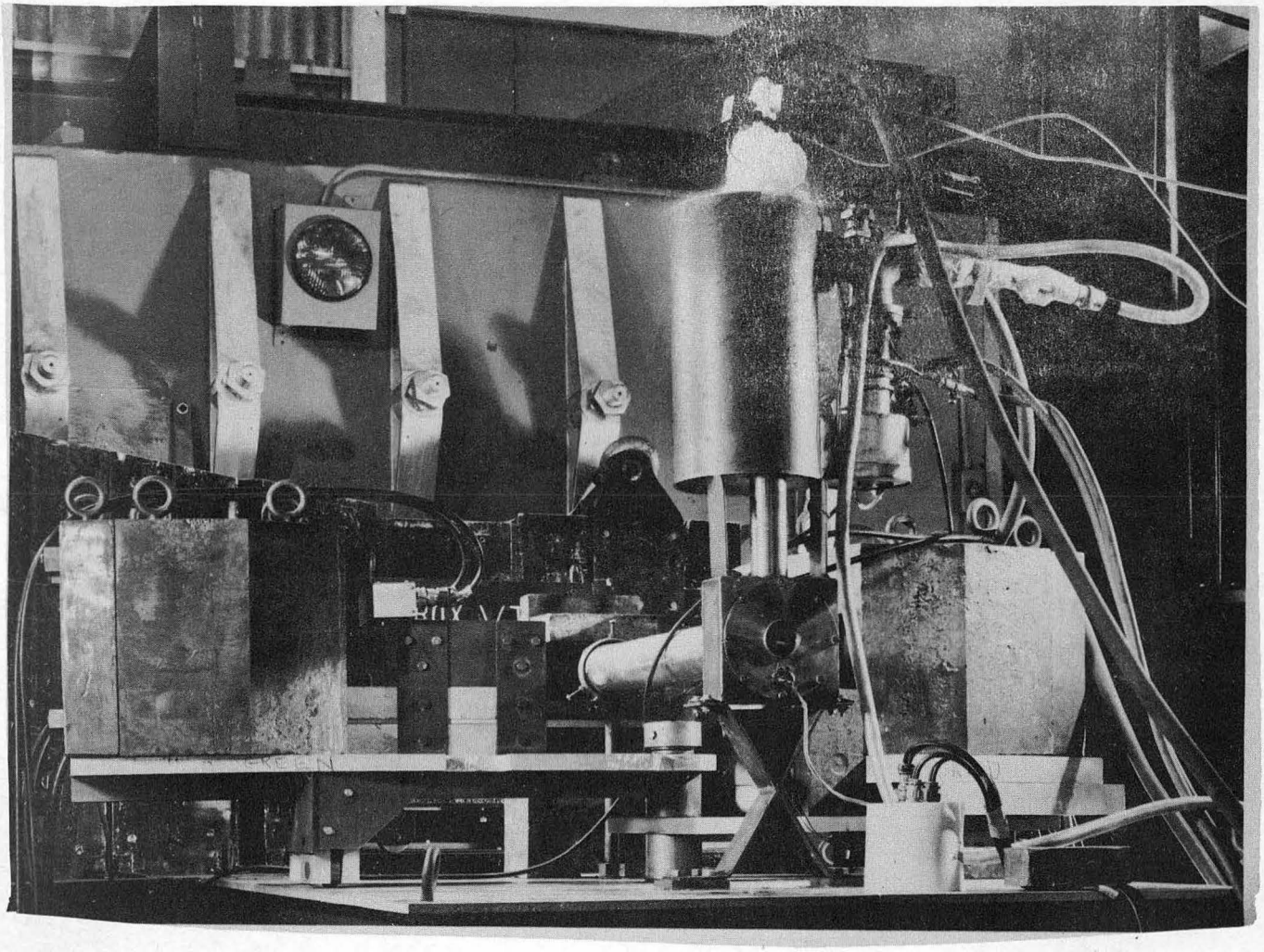

Fig. 4

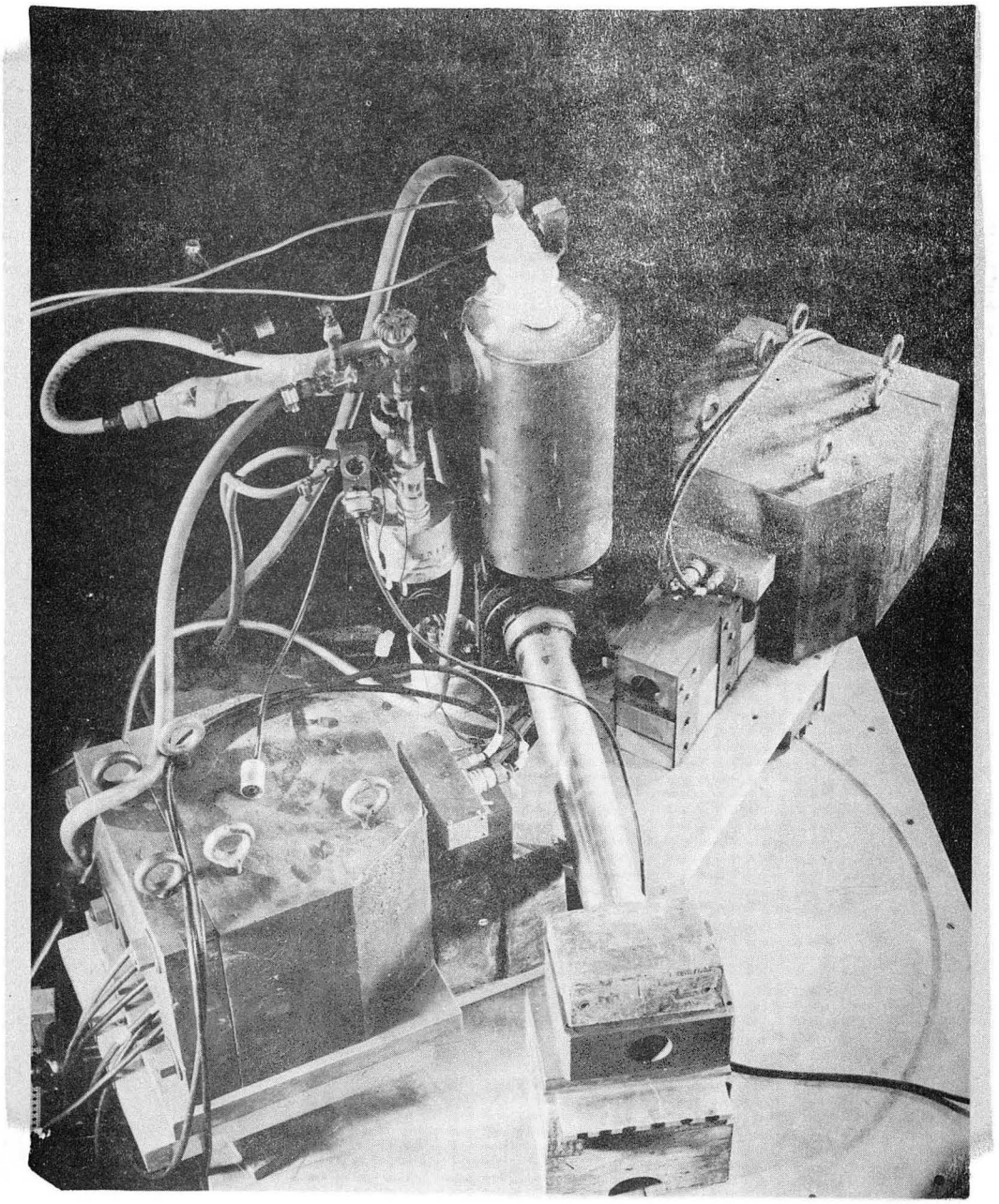

Fig. 5

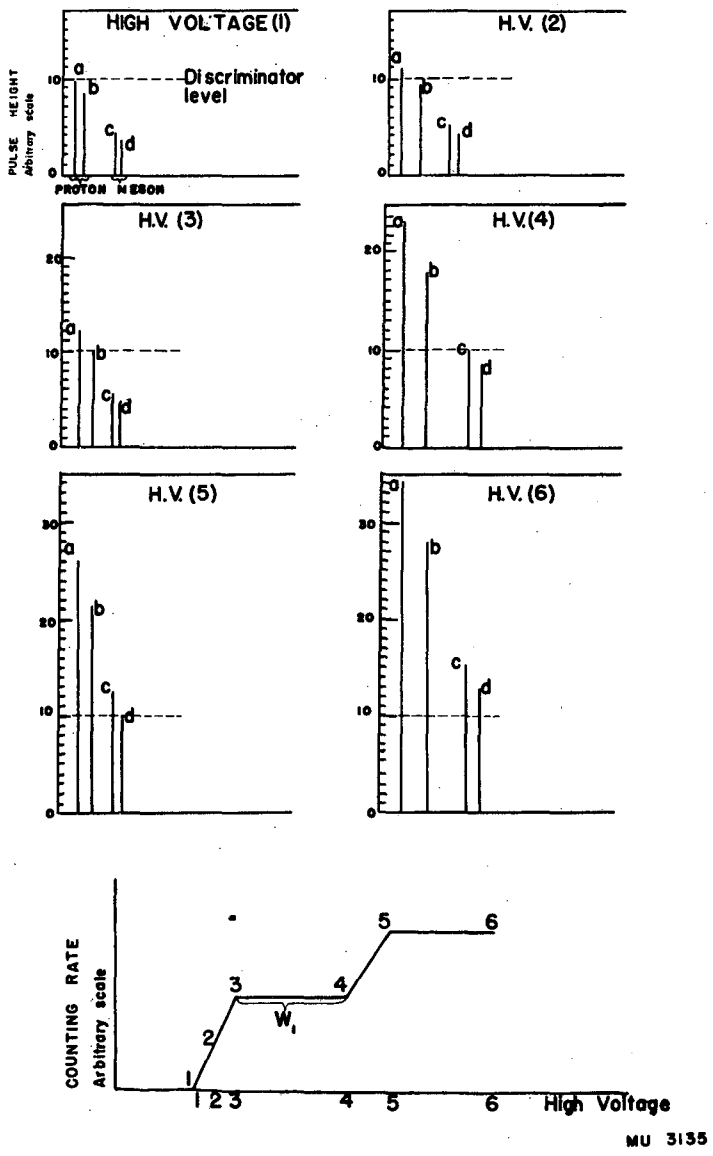
HIGH VOLTAGE (1)
Discriminator level
PULSE HEIGHT Arbitrary scale
PROTON
MESON
H.V. (2)
H.V. (3)
H.V. (4)
H.V. (5)
H.V. (6)
a
b
c
d
COUNTING RATE Arbitrary scale
1
2
3
4
5
6
W_1
High Voltage
MU 3135

Fig. 6

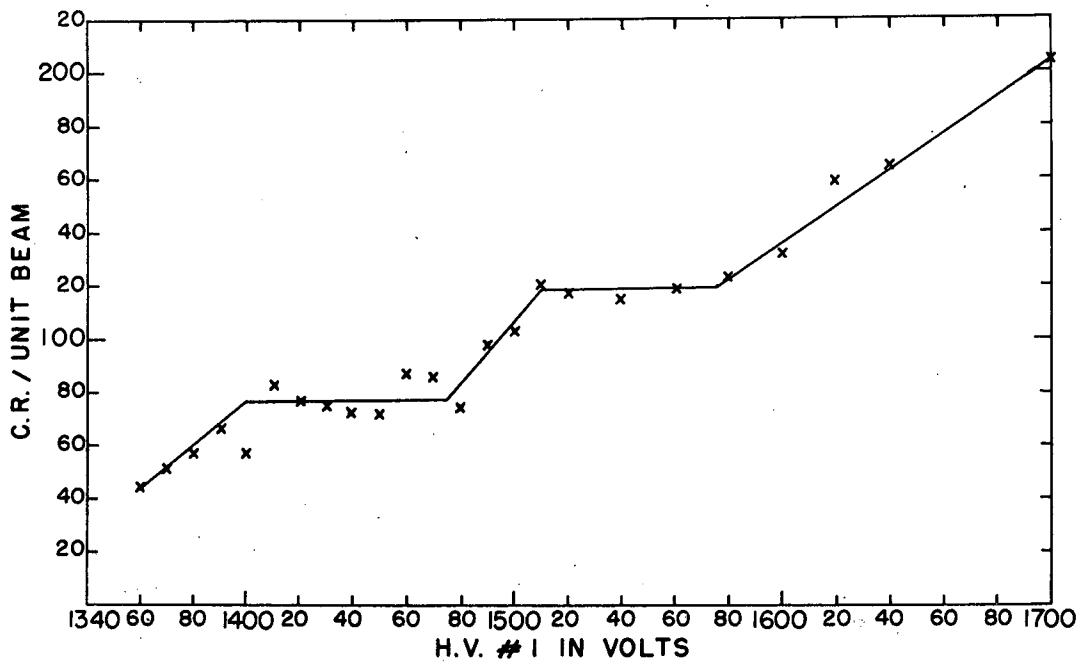

SYNCHROTRON 324-MEV BREMSSTRAHLUNG YIELD VS. P. M. H. V.

MU 3100

Fig. 7

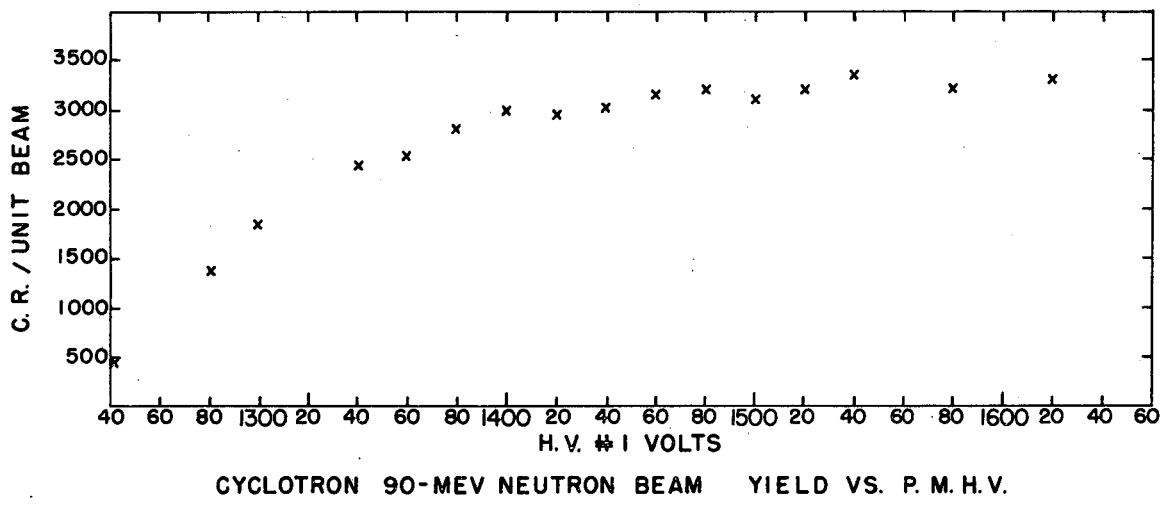
C. R. / UNIT BEAM
3500
3000
2500
2000
1500
1000
500
40 60 80 1300 20 40 60 80 1400 20 40 60 80 1500 20 40 60 80 1600 20 40 60
H.V. #1 VOLTS
CYCLOTRON 90-MEV NEUTRON BEAM YIELD VS. P. M. H.V.
MU 3101

Fig. 8

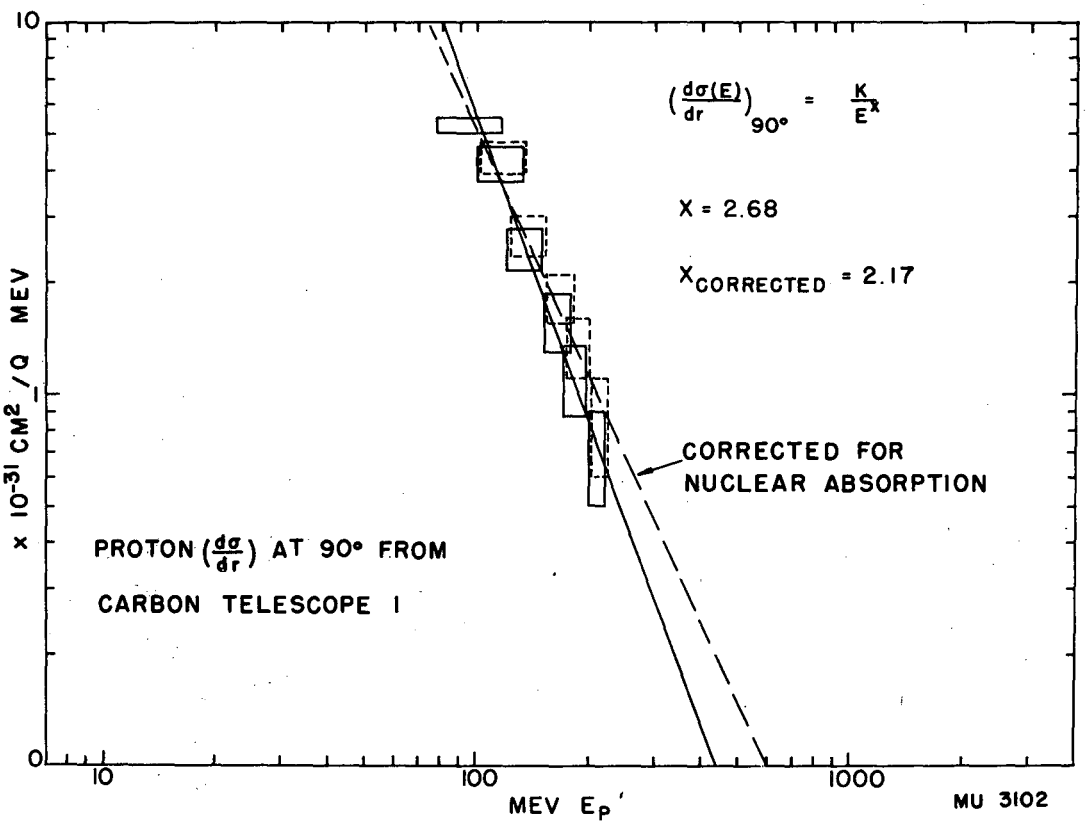
10
0
$\times 10^{-31}$ CM^2/Q MEV
$\left(\frac{d\sigma(E)}{dr}\right)_{90°} = \frac{K}{E^X}$
X = 2.68
$X_{CORRECTED}$ = 2.17
CORRECTED FOR
NUCLEAR ABSORPTION
PROTON $\left(\frac{d\sigma}{dr}\right)$ AT 90° FROM
CARBON TELESCOPE I
10
100
1000
MEV E_P
MU 3102

Fig. 9

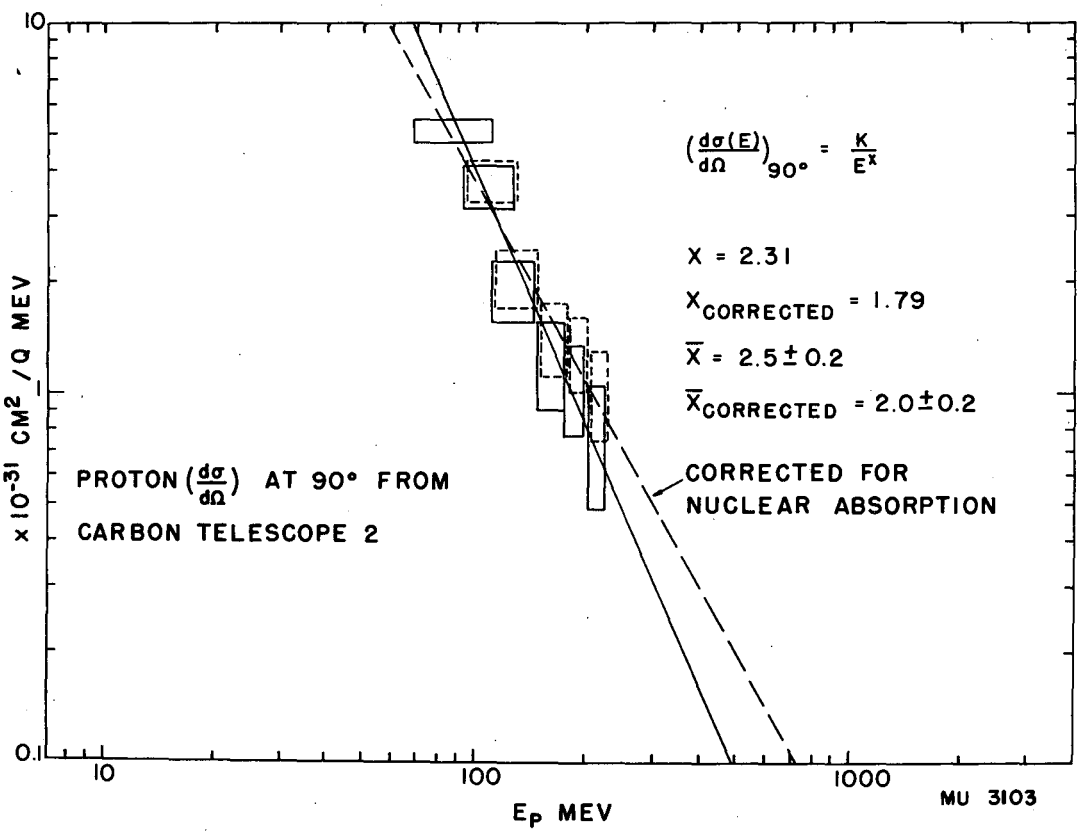
10
1
0.1
x 10⁻³¹ CM² / Q MEV
10
100
1000
Eₚ MEV
MU 3103
(dσ(E)/dΩ)₉₀° = K/E^X
X = 2.31
X_CORRECTED = 1.79
X̄ = 2.5 ± 0.2
X̄_CORRECTED = 2.0 ± 0.2
PROTON (dσ/dΩ) AT 90° FROM
CARBON TELESCOPE 2
CORRECTED FOR
NUCLEAR ABSORPTION

Fig. 10

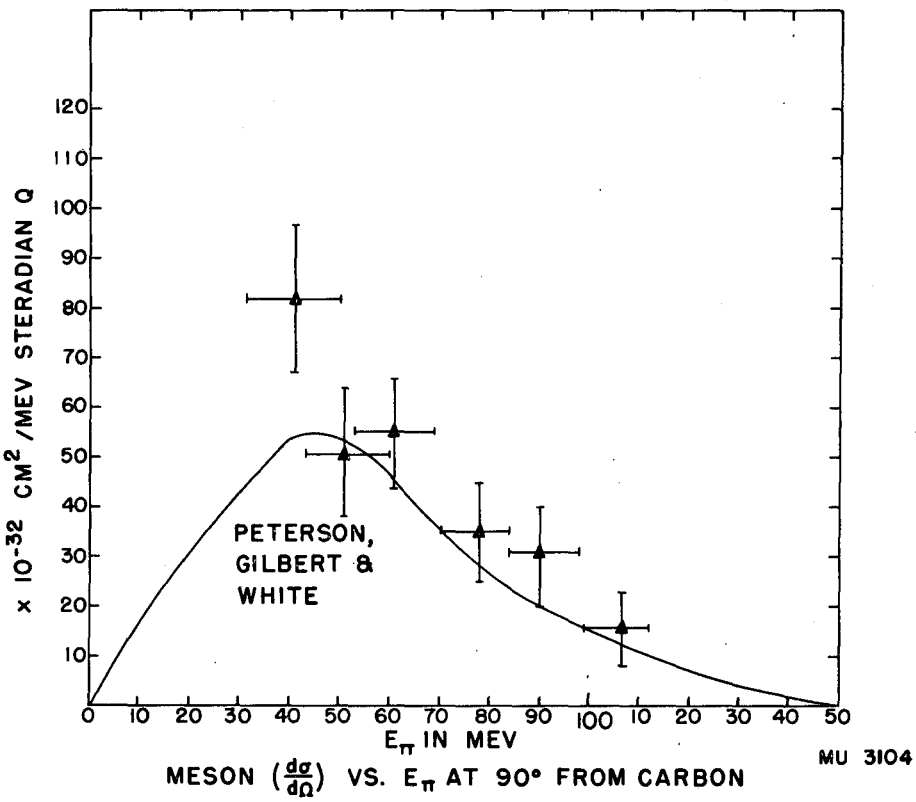
x 10⁻³² CM² /MEV STERADIAN Ω
120
110
100
90
80
70
60
50
40
30
20
10
0 10 20 30 40 50 60 70 80 90 100 10 20 30 40 50
Eπ IN MEV
PETERSON,
GILBERT &
WHITE
MU 3104
MESON (dσ/dΩ) VS. Eπ AT 90° FROM CARBON

Fig. 11

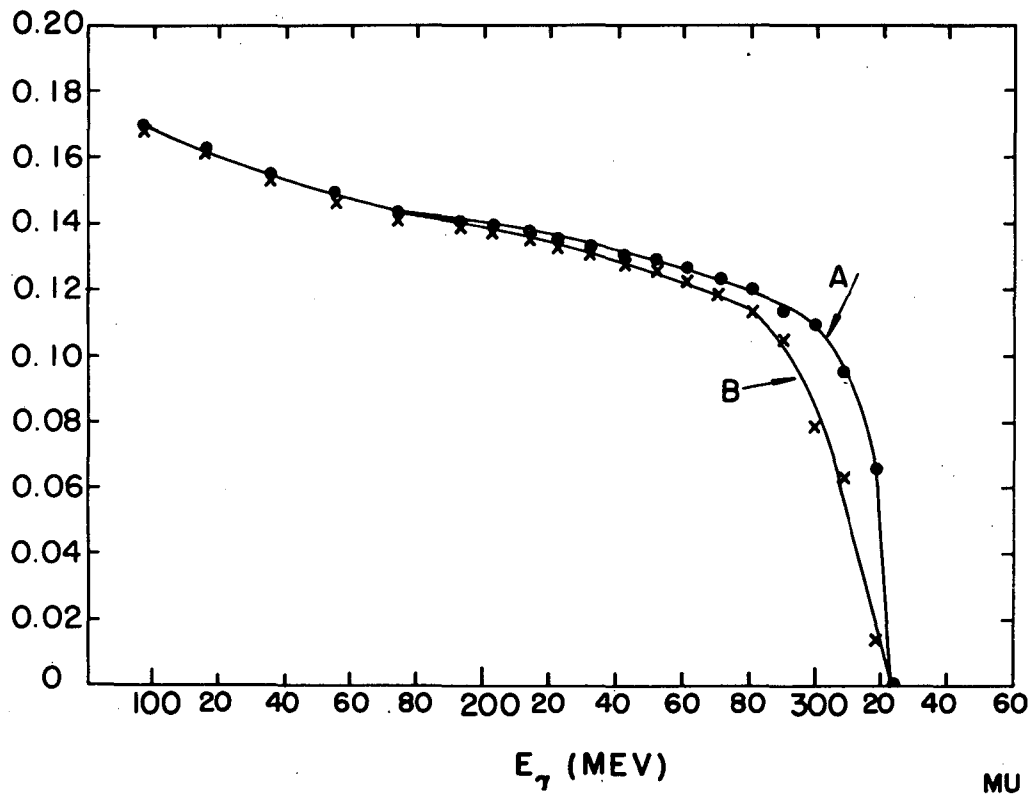
0.20
0.18
0.16
0.14
0.12
0.10
0.08
0.06
0.04
0.02
0
100 20 40 60 80 200 20 40 60 80 300 20 40 60
E_γ (MEV)
A
B
MU 3105

Fig. 12

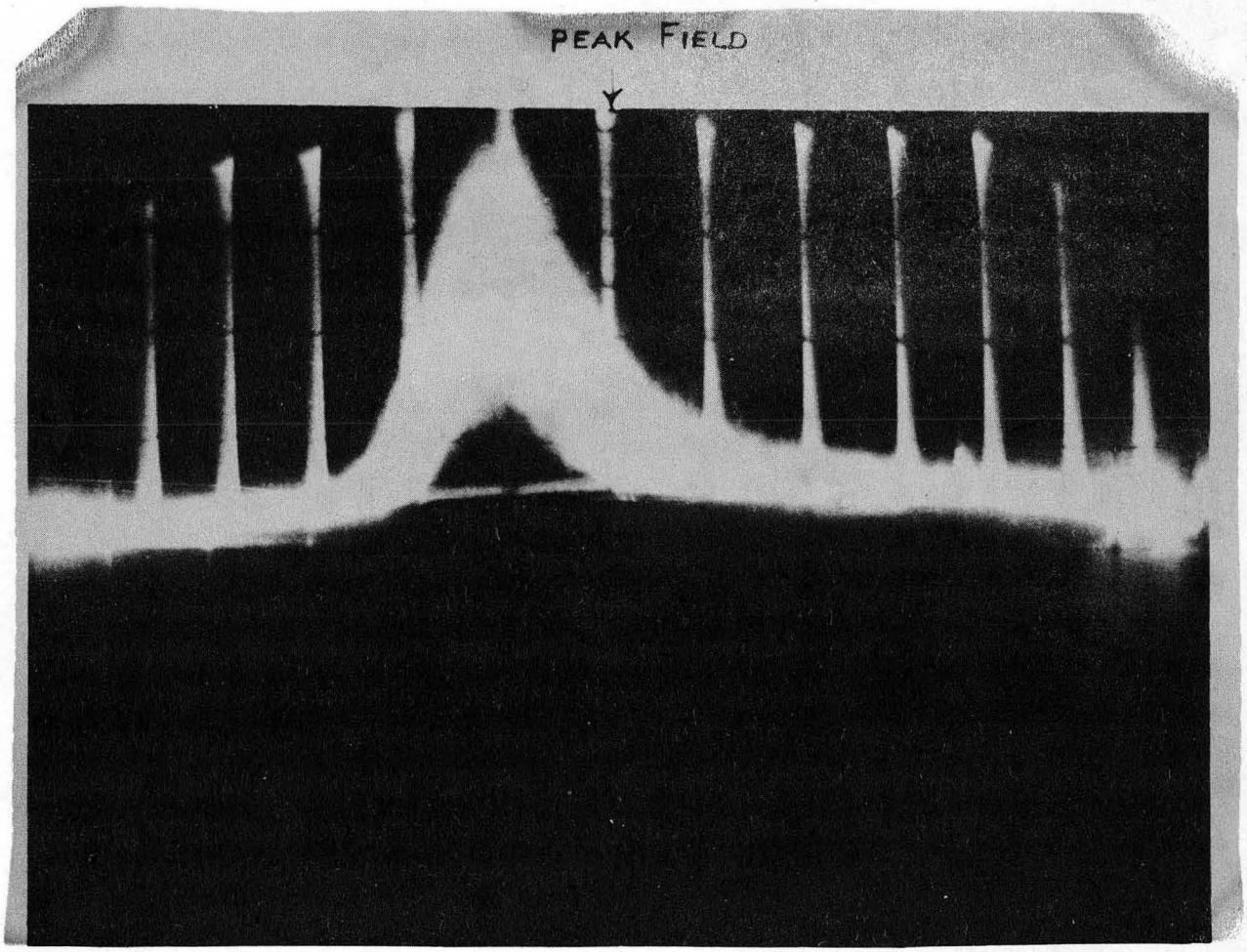

Fig. 13

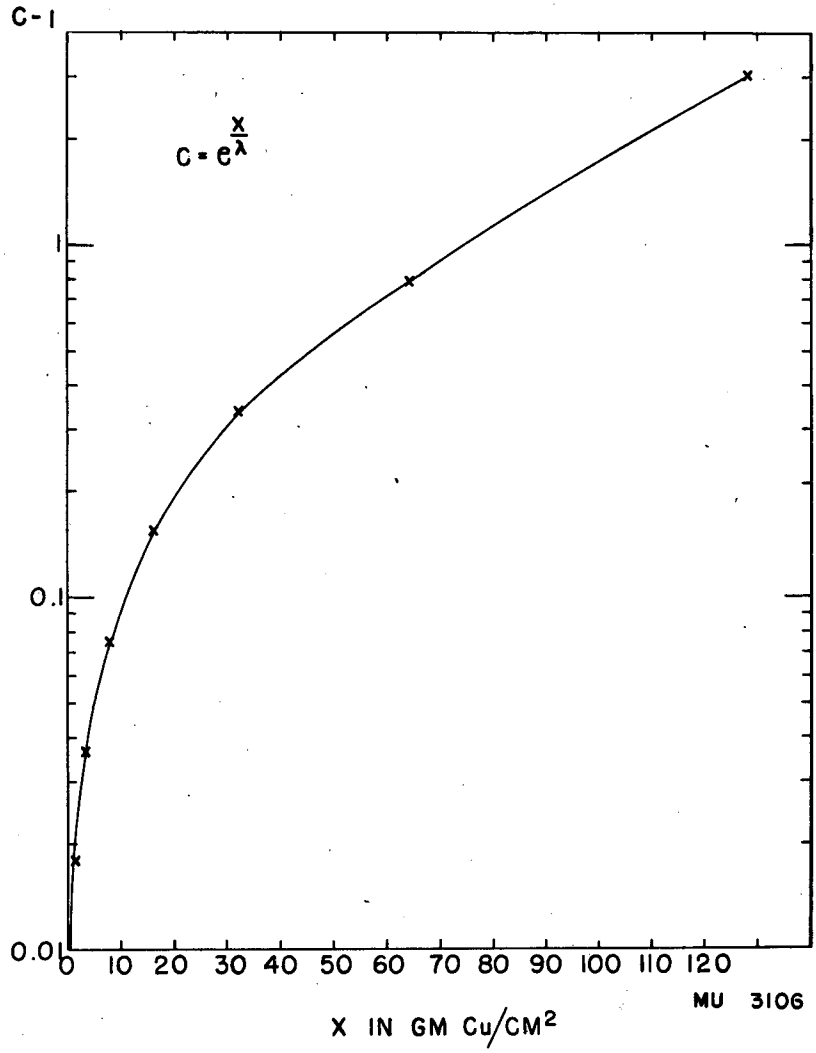
C - 1
$C = e^{\frac{X}{\lambda}}$
1
0.1
0.01
0 10 20 30 40 50 60 70 80 90 100 110 120
MU 3106
X IN GM Cu/CM²

Fig. 14

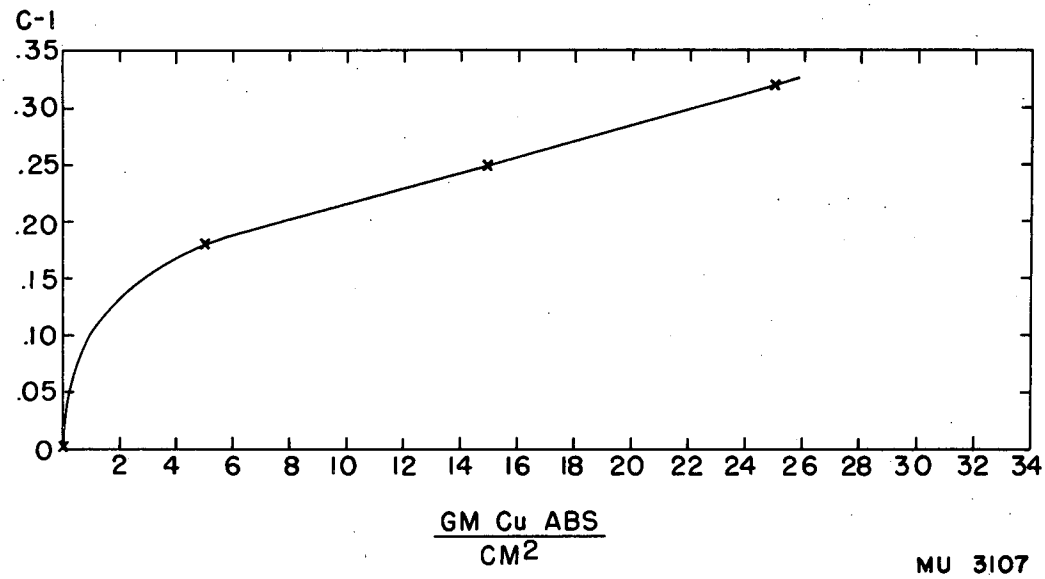

MULTIPLE SCATTERING CORRECTION

Fig. 15

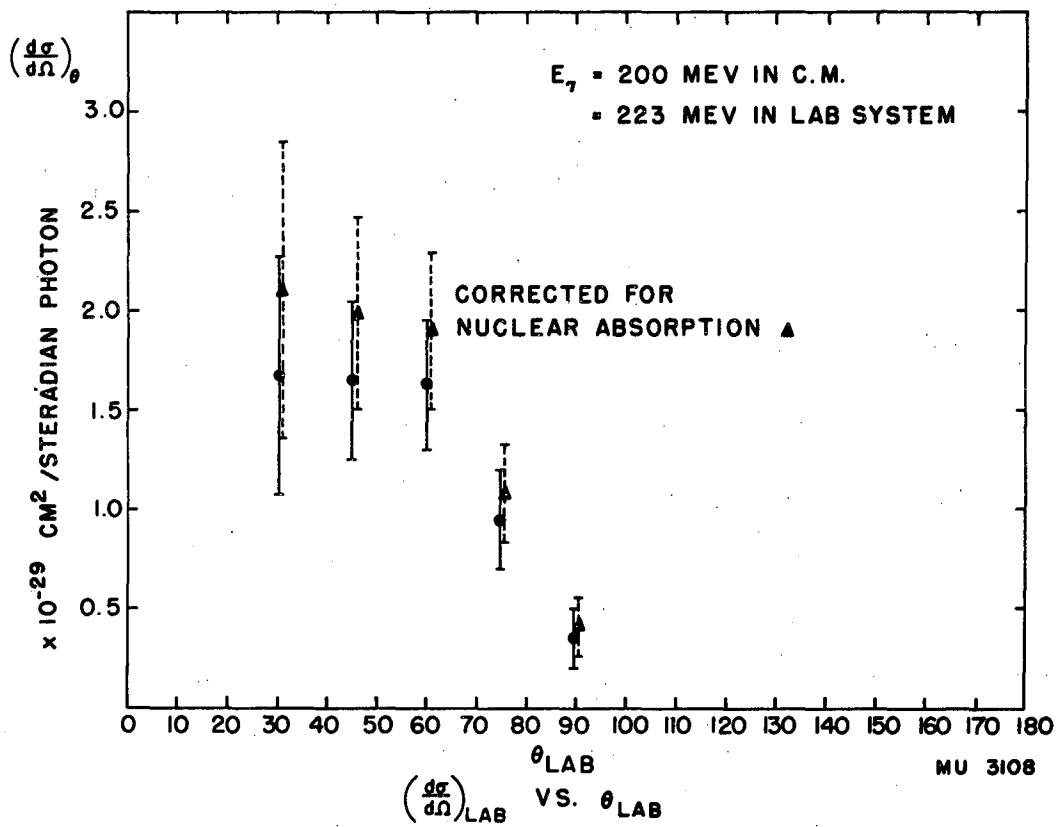
$\left(\frac{d\sigma}{d\Omega}\right)_\theta$
E_γ = 200 MEV IN C.M.
= 223 MEV IN LAB SYSTEM
CORRECTED FOR
NUCLEAR ABSORPTION ▲
x 10^{-29} CM^2 /STERADIAN PHOTON
3.0
2.5
2.0
1.5
1.0
0.5
0 10 20 30 40 50 60 70 80 90 100 110 120 130 140 150 160 170 180
θ_{LAB}
MU 3108
$\left(\frac{d\sigma}{d\Omega}\right)_{LAB}$ VS. θ_{LAB}

Fig. 16

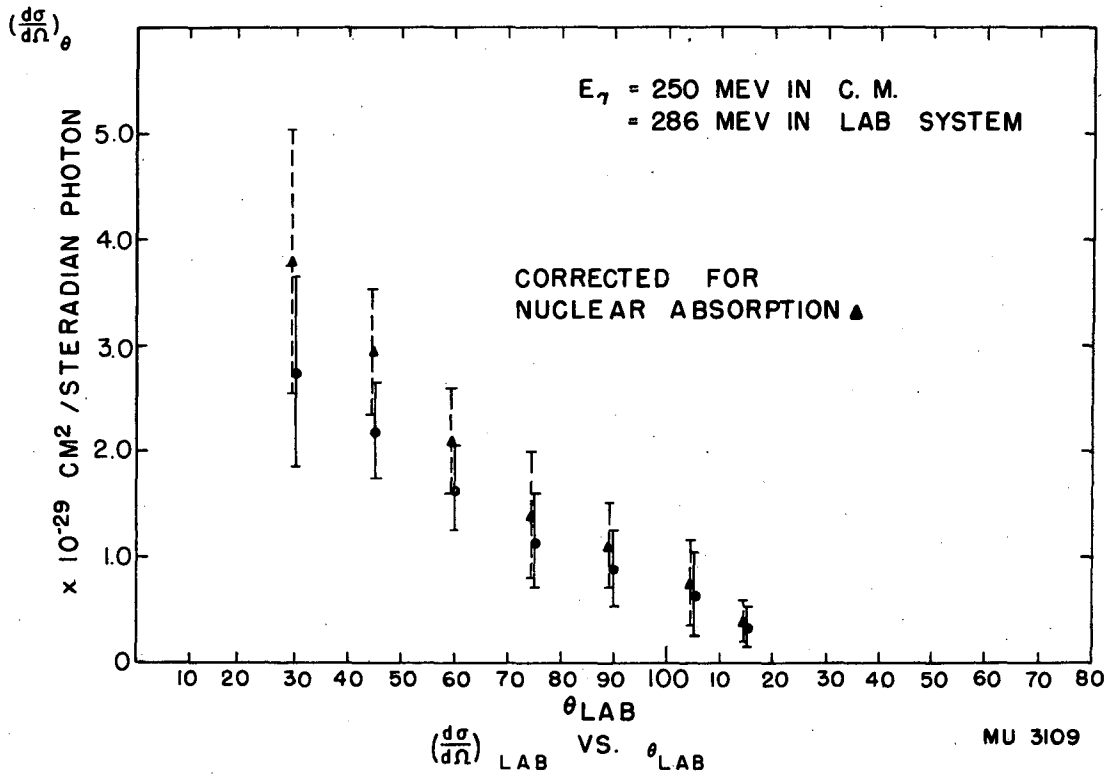
$(\frac{d\sigma}{d\Omega})_\theta$
E_γ = 250 MEV IN C. M.
= 286 MEV IN LAB SYSTEM
CORRECTED FOR
NUCLEAR ABSORPTION ▲
x 10^{-29} CM^2 /STERADIAN PHOTON
0
1.0
2.0
3.0
4.0
5.0
10 20 30 40 50 60 70 80 90 100 10 20 30 40 50 60 70 80
θLAB
$(\frac{d\sigma}{d\Omega})_{LAB}$ VS. θ_{LAB}
MU 3109

Fig. 17

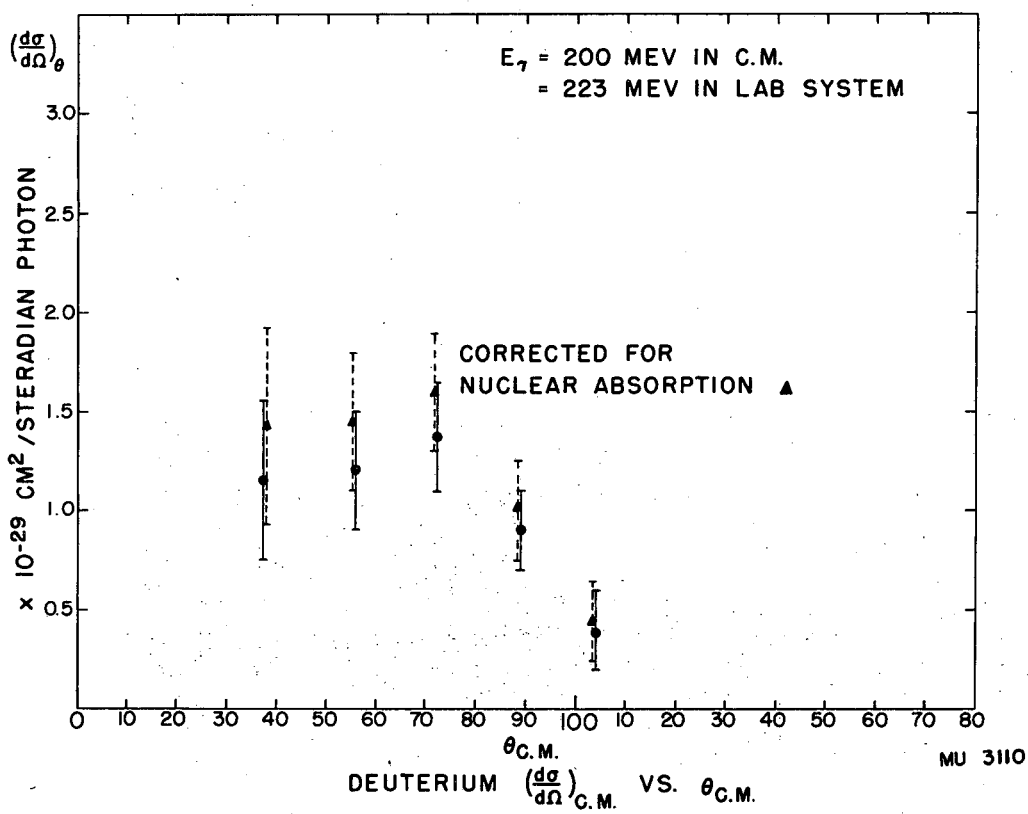
$(\frac{d\sigma}{d\Omega})_\theta$
E_γ = 200 MEV IN C.M.
= 223 MEV IN LAB SYSTEM
CORRECTED FOR
NUCLEAR ABSORPTION ▲
× 10-29 CM2/STERADIAN PHOTON
3.0
2.5
2.0
1.5
1.0
0.5
0 10 20 30 40 50 60 70 80 90 100 10 20 30 40 50 60 70 80
$\theta_{C.M.}$
MU 3110
DEUTERIUM $(\frac{d\sigma}{d\Omega})_{C.M.}$ VS. $\theta_{C.M.}$

Fig. 18

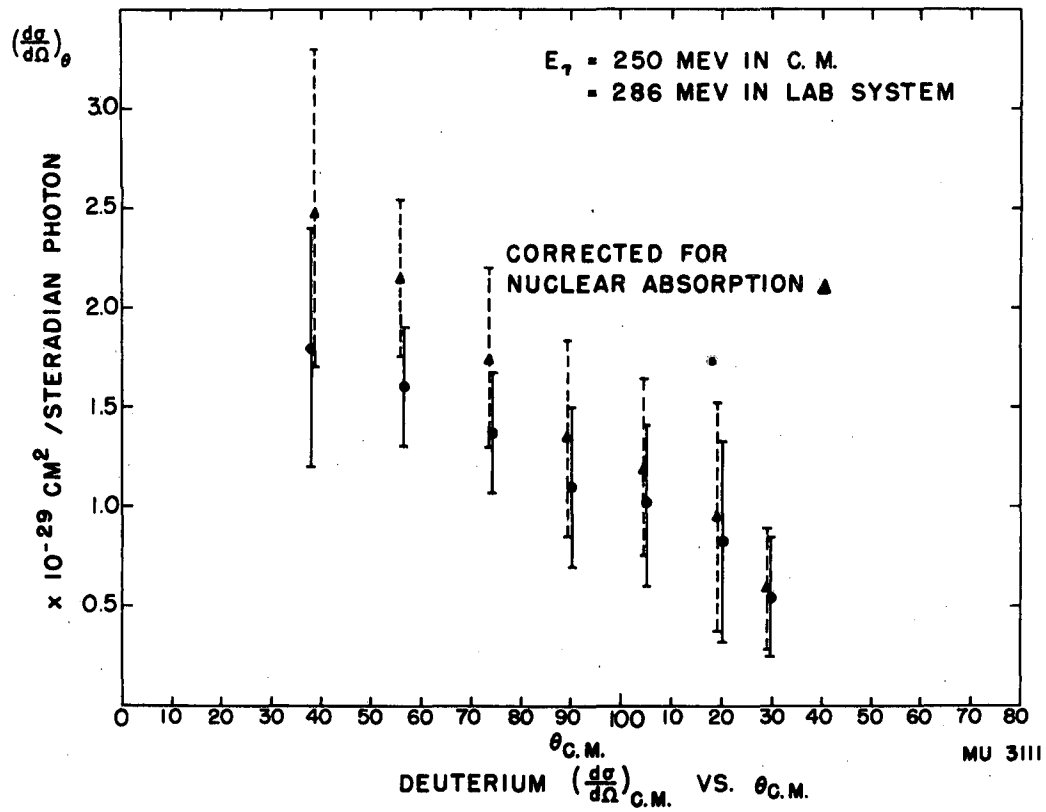
$(\frac{d\sigma}{d\Omega})_\theta$
E_γ = 250 MEV IN C. M.
= 286 MEV IN LAB SYSTEM
CORRECTED FOR
NUCLEAR ABSORPTION ▲
× 10^{-29} CM^2 /STERADIAN PHOTON
3.0
2.5
2.0
1.5
1.0
0.5
0 10 20 30 40 50 60 70 80 90 100 10 20 30 40 50 60 70 80
$\theta_{C.M.}$
MU 3111
DEUTERIUM $(\frac{d\sigma}{d\Omega})_{C.M.}$ VS. $\theta_{C.M.}$

Fig. 19

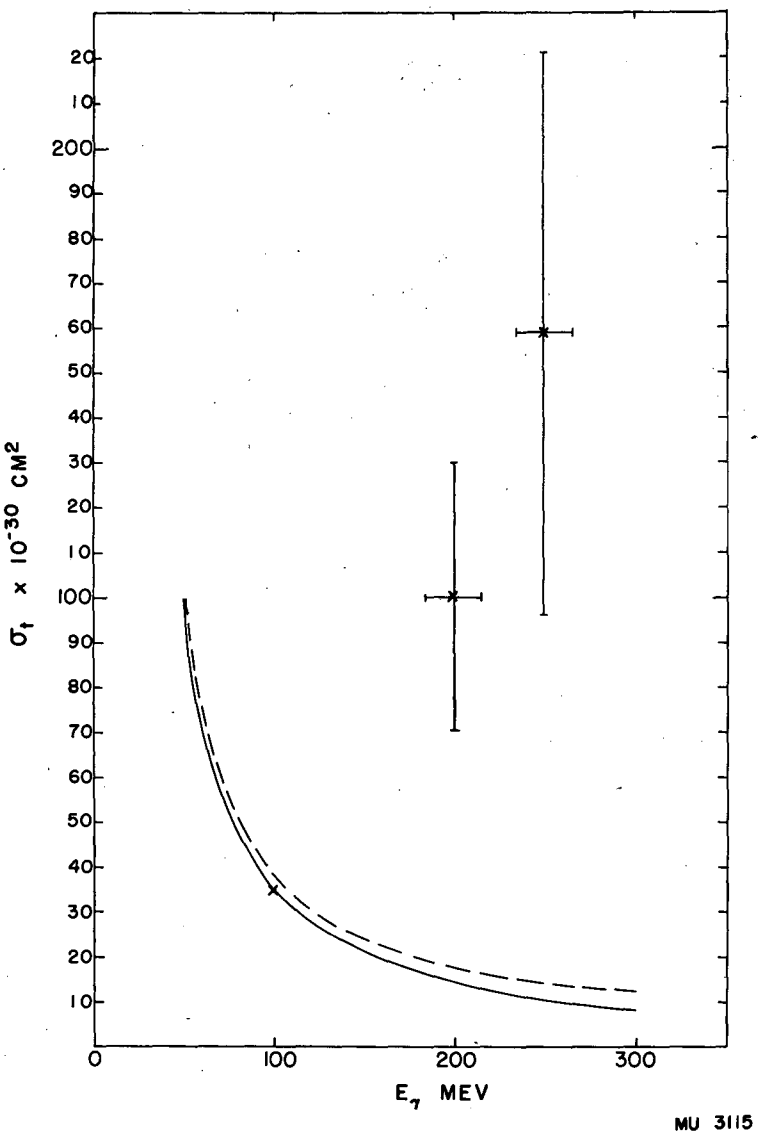

Fig. 20.

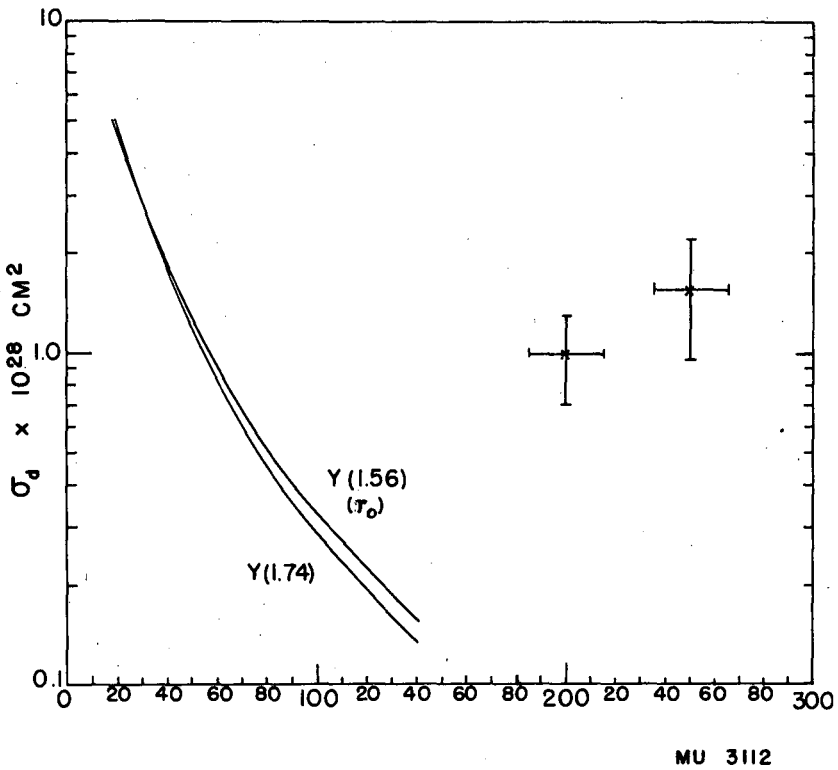
10
1.0
0.1
σ_d x 10^{28} CM^2
Y (1.56)
(r_o)
Y(1.74)
0
20
40
60
80
100
20
40
60
80
200
20
40
60
80
300
MU 3112

Fig. 21

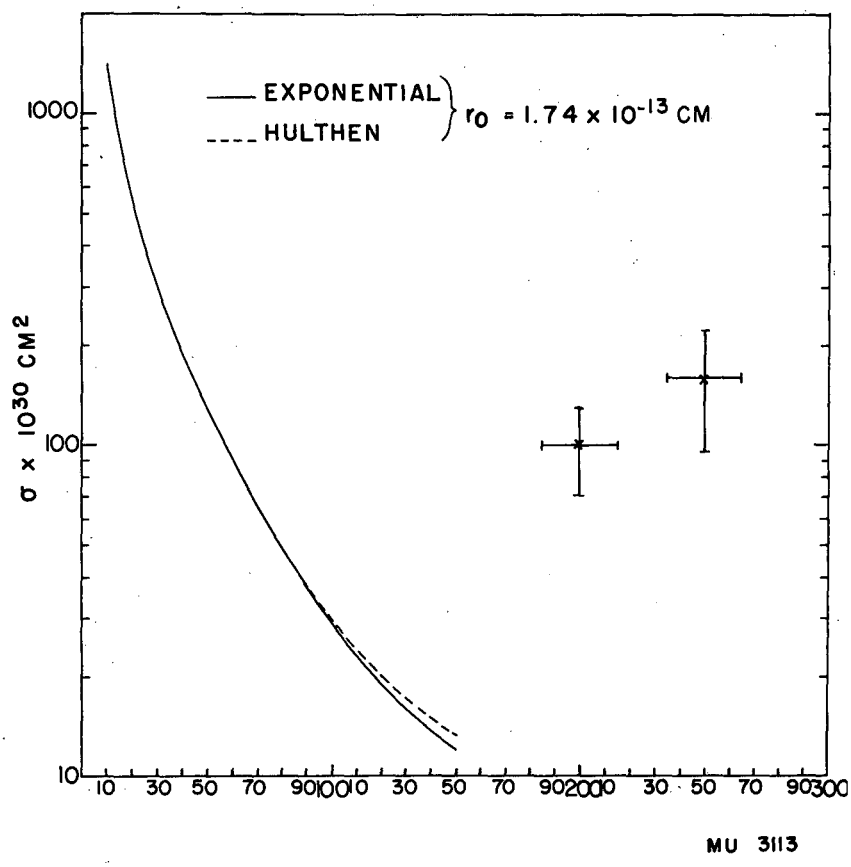
EXPONENTIAL
HULTHEN
$r_0 = 1.74 \times 10^{-13}$ CM
$\sigma \times 10^{30}$ CM^2
1000
100
10
10 30 50 70 90 100 10 30 50 70 90 200 10 30 50 70 90 300
MU 3113

Fig. 22

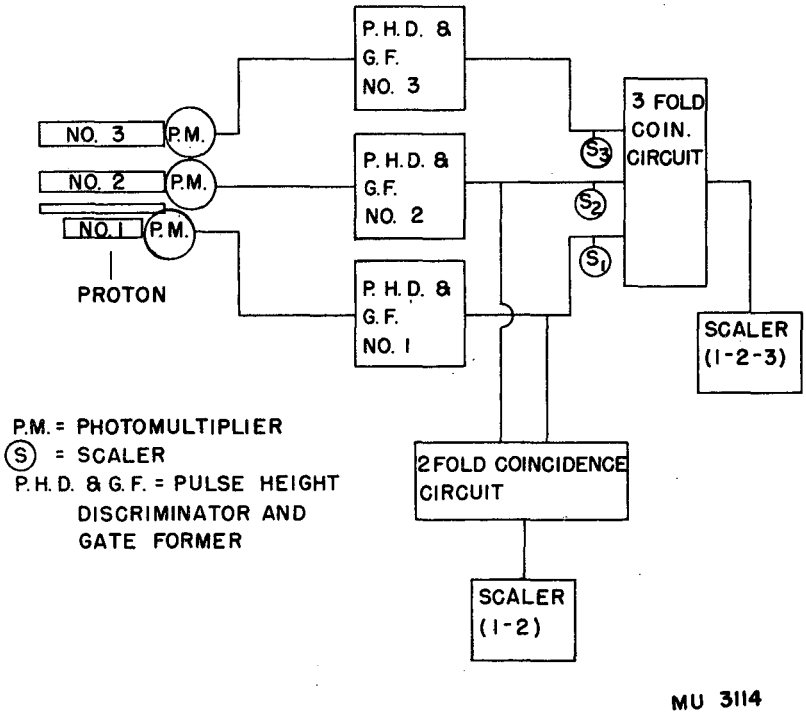
P. H. D. & G. F. NO. 3
P. H. D. & G. F. NO. 2
P. H. D. & G. F. NO. 1
3 FOLD COIN. CIRCUIT
NO. 3
NO. 2
NO. 1
P.M.
P.M.
P.M.
PROTON
S3
S2
S1
SCALER (1-2-3)
2 FOLD COINCIDENCE CIRCUIT
SCALER (1-2)
P.M. = PHOTOMULTIPLIER
(S) = SCALER
P. H. D. & G. F. = PULSE HEIGHT DISCRIMINATOR AND GATE FORMER
MU 3114

Fig. 23